A mangrove lifecycle ecosystem analysis and forecasting (LEAF) model

Dunlop, Thomas; Felder, Stefan; Glamore, William

DOI
10.1016/j.envsoft.2025.106619

Publication date
2025

Document Version
Final published version

Published in
Environmental Modelling and Software

Environmental Modelling and Software 193 (2025) 106619

Contents lists available at ScienceDirect

Environmental Modelling and Software

journal homepage: www.elsevier.com/locate/envsoft

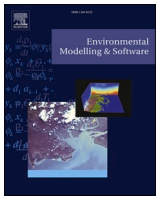

A mangrove lifecycle ecosystem analysis and forecasting (LEAF) model

Thomas Dunlop [a,b,*], Stefan Felder [a], William Glamore [a]

[a] Water Research Laboratory, School of Civil and Environmental Engineering, UNSW Sydney, Sydney, NSW, Australia
[b] Department of Hydraulic Engineering, Delft University of Technology, 2600, GA, Delft, the Netherlands

ARTICLE INFO

Keywords:
Avicennia marina
Biophysical modelling
Design guidance
Forest dynamics
Mangrove
Nature-based solutions
Restoration

ABSTRACT

Mangroves are recognised for the ecosystem services they provide, yet practitioners lack guidance for quantifying these services over time. To overcome this knowledge gap, this study developed a numerical tool, the mangrove Lifecycle Ecosystem Analysis and Forecasting (LEAF) model, that simulates the growth and mortality of mangroves across all lifecycle stages (seedling to senescence). To test model functionality, the LEAF model (version 1.0, dated January 31, 2025) was coupled to Delft3D Flexible Mesh, where individual mangrove size, impacts of extreme events, biomass, and coastal protection parameters were monitored. Cross-shore mangrove distribution was successfully predicted in four estuary typologies over temporal domains of 5–12 years. Sensitivity analyses revealed the timing and duration of the fruiting window, inundation free period, and inundation depth as critical to forest development. Results highlight the need for field data acquisition to target these thresholds, further validate mangrove growth, and expand the model to other species and locations worldwide.

1. Introduction

Mangroves provide a variety of critical ecosystem services, such as supporting habitats (Miedema Brown and Anand, 2022), fisheries (Faunce and Serafy, 2006), and providing shoreline protection by dampening waves (Quartel et al., 2007) and accumulating sediment (Lovelock et al., 2011). In recognition of these services, mangroves are increasingly being prioritised over grey infrastructure because of their potential to enhance biodiversity (Mumby et al., 2004) while mitigating climate change through carbon sequestration (Alongi, 2014), attenuating storm energy (Menéndez et al., 2020), and raising bed levels via sediment trapping (Lovelock et al., 2011). To determine if and when these co-benefits are realised, further understanding of how mangrove forests develop and function over time is needed (Dunlop et al., 2023).

Quantifying the ecosystem services of a mangrove forest requires a detailed understanding of the mangrove lifecycle (Dunlop et al., 2023). Predicting how mangrove forests respond to varying climatic conditions and hydrodynamic processes can help practitioners evaluate the long-term viability of mangroves as Nature-based Solutions (NbS). These lifecycle predictions can complement research on mangrove capacity to withstand acute stressors (Henderson and Glamore, 2024a; Menéndez et al., 2020) or to indicate the potential success of various restoration methods (van Bijsterveldt et al., 2022). For example, a lifecycle approach may predict whether a shoreline is suitable for mangrove establishment or whether the established mangroves can reduce erosional forces. In this regard, mangrove growth may be hindered or sustained by changes during its lifecycle due to potential alterations in bed level (Ellison, 1999), water level (Choy and Booth, 1994), or bed shear stresses (Balke et al., 2011).

Predicting ecosystem growth has previously been explored by coupling biophysical processes scripted in coding software such as MATLAB (van Maanen et al., 2015; Xie et al., 2020, 2022) and Python (Beselly et al., 2023; Caponi et al., 2023; Dzimballa et al., 2025; Hendrickx et al., 2021; Gijsman et al., 2024a) via hydro-morphodynamic modelling packages like Delft3D. This coupling process has been used to predict how mangrove forests respond to environmental change, such as sea level rise (Best et al., 2021; Xie et al., 2020). While alterations to the nearshore hydrodynamics can influence the establishment, growth, mortality, and recovery phases of the ecosystem lifecycle (Dunlop et al., 2023), current biophysical models have not modelled all lifecycle stages or evaluated the sensitivity of biophysical parameters for mangroves on an individual basis. In previous research, the dynamics of individual mangrove trees across lifecycle stages have focused on the critical establishment and growth phases of mangrove forest development by incorporating competition stresses (Beselly et al., 2023), and propagule abscission and dispersal (Gijsman et al., 2024a). Beyond the establishment phase, mangrove dynamics have been evaluated by calculating the growth and decay of the mangrove population (rather than individuals)

* Corresponding author. Water Research Laboratory, School of Civil and Environmental Engineering, UNSW Sydney, 110 King St, Manly Vale NSW 2093, Australia.
E-mail address: t.dunlop@unsw.edu.au (T. Dunlop).

https://doi.org/10.1016/j.envsoft.2025.106619
Received 14 February 2025; Received in revised form 9 July 2025; Accepted 9 July 2025
Available online 12 July 2025

caused by modified growth rates, establishment densities, and the impacts of inundation and flow (Best et al., 2021). However, this approach does not consider diversity in mangrove size and age, where, for example, individual mangroves at the seaward edge of the forest may be exposed to higher bed shear stresses from currents and waves, and at locations where seedlings may grow in amongst more mature trees.

Understanding the response of individual mangroves across the lifecycle to extreme events, including inundation, desiccation, erosion, and burial, is critical to predicting how forest size, extent, and health changes over time. However, this requires long-term field and laboratory measurements to accurately determine the threshold magnitudes and durations that cause stress and mortality. To this end, current models have focused on site-specific studies where mangrove extent and age-height relationships in response to sediment deposition (Beselly et al., 2023), or the capacity for mangroves to influence sediment accretion (Gijsman et al., 2024b), can be observed and utilised for model validation. Limited research has been undertaken to validate individual based mangrove models over various spatial and temporal domains. Further, no models currently exist where practitioners can update a user-friendly tool to monitor biophysical processes and utilise parameter relationships derived from field observations and laboratory experiments to evaluate the success of mangrove restoration in a range of environmental settings.

To advance current approaches, an individual-based mangrove lifecycle model has been developed in Python and coupled to Delft3D Flexible Mesh. This mangrove Lifecycle Ecosystem Analysis and Forecasting (LEAF) model (version 1.0, dated January 31, 2025) can predict the long-term change of existing or restored mangrove forests, allowing practitioners to simulate the trajectory of mangrove forests prior to planting or undertaking site remediation works. The LEAF model predicts how individual mangroves will respond to stressor events including extreme high and low water levels, sedimentation, and erosion, based on ecological and engineering parameters derived from field data and laboratory experiments in academic literature. When projected at a local site, the LEAF model can be used to quantify potential restoration outcomes including forest attributes such as stem and root size, carbon storage via biomass calculations, coastal protection via drag coefficients, projected forested areas and volumes, and bed level change. Guidance notes accompany the model code to provide practitioners with an easy-to-use tool for predicting mangrove ecosystem response under a range of estuarine and coastal settings.

2. Materials and methods

2.1. Modelling framework

The biophysical LEAF model was written in Python (version 3.10) and forms the basis for the mangrove design tool presented herein.

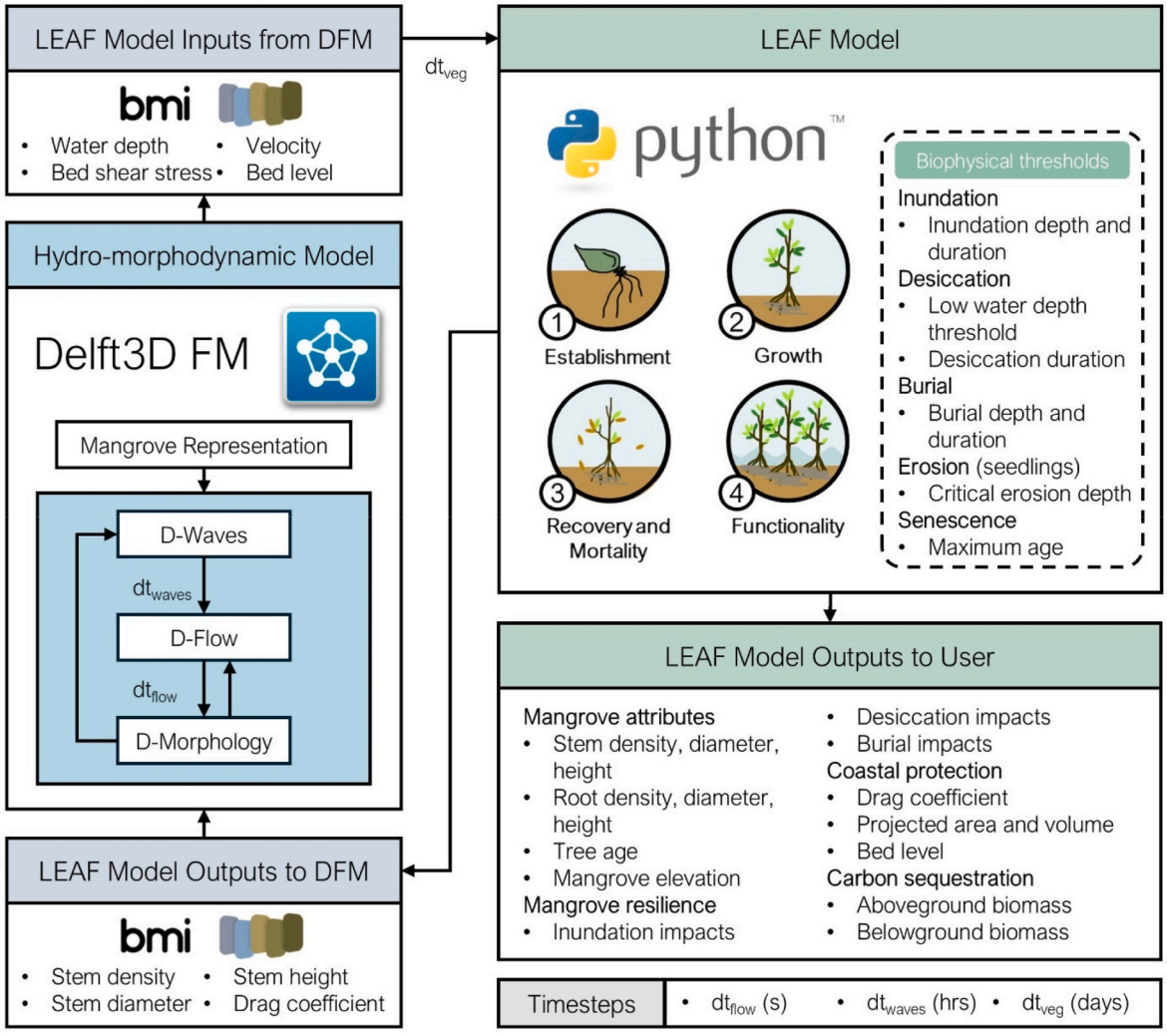

Fig. 1. The modelling workflow, including the coupling of the LEAF model developed in Python with the hydro-morphodynamic model in Delft3D Flexible Mesh via the BMI interface.

Version 1.0 of the LEAF model, LEAF (v.1.0), is available at https://github.com/DunlopT/LEAF. This biophysical model was developed using a constant feedback loop between the biological and hydro-morphodynamic processes. The Python script was coupled to the D-Flow and D-Waves modules (Fig. 1) from the Delft3D Flexible Mesh (DFM) hydrodynamic model suite (version 2021.03) (Deltares, 2021). The DFM Suite is a series of process-based modules that resolve the shallow water equations on unstructured grids to determine the resultant hydrodynamic processes (D-Flow) (Kernkamp et al., 2011), simulate and compute the evolution and propagation of waves with the SWAN (Simulating Waves Nearshore) model (D-Waves) (Deltares, 2020b), resolve the advection-diffusion equation for suspended sediment transport, and compute bed erosion within an estuarine setting (D-Morphology) (Deltares, 2020a).

For the feedback loop, the Python script in LEAF (v.1.0) was coupled to the DFM model using the Basic Model Interface (BMI) module (Hutton et al., 2020), where parameters are exchanged at the beginning of each hydro-morphodynamic and mangrove timestep, respectively. Variables such as bed levels, maximum water depths, flow velocities, and bed shear stresses are retrieved by the Python code from the DFM model at the end of each hydro-morphodynamic timestep. These variables are then used to evaluate changes across a 4-stage mangrove lifecycle approach (Dunlop et al., 2023) using a range of biophysical thresholds corresponding to the stress and mortality of mangroves because of inundation, desiccation, burial, and erosion pressures. The evolution of the mangrove ecosystem is quantified in terms of the physical parameters required for the modified Baptist bulk roughness formulae for vegetation (Baptist et al., 2007), namely the stem height, diameter, density, and bulk drag coefficient. These parameters are exchanged with the DFM model at the end of the biophysical timestep in LEAF (v.1.0) and before the next hydro-morphodynamic timestep. At user-defined intervals, these mangrove attributes are exported and can be observed by the user to track the trajectory of mangrove restoration. Mangrove resilience to hydro-morphodynamic impacts, and the degree to which the mangrove forest can provide the ecosystem services of coastal protection and carbon sequestration are also available to the user. A summary of the modelling workflow is presented in Fig. 1.

LEAF (v.1.0) is designed for the mangrove species *Avicennia marina*, one of the most prominent species worldwide (Duke, 1991). The root structure of *Avicennia marina* comprises pneumatophores, which are aerial, pencil-shaped roots, that can promote sediment deposition in the landward areas of mangrove forests (Deitrick et al., 2023) and increase growth in periods of inundation (Toma et al., 1991) and burial (Okello et al., 2020) to maximise oxygen intake for the mangrove. Data for this species are more readily available than other species and, thereby, *Avicennia marina* presents a detailed starting point to establish an individual-based mangrove model and to expand on the current knowledge in mangrove modelling (Beselly et al., 2023; Gijsman et al., 2024a).

2.2. Model logic

2.2.1. Overview

To develop LEAF (v.1.0), the logical processes for the dynamics of an *Avicennia marina* mangrove forest were integrated into a Python script. This section presents an overview of the core logic behind the model, with subsequent sections describing the underlying principles and detailed logical processes of the four developmental stages included in the model, based on the conceptual approach of Dunlop et al. (2023): 1) Establishment, 2) Growth, 3) Recovery and mortality, and 4) Functionality.

In LEAF (v.1.0), individual mangrove stem and pneumatophore dynamics are updated across two main evolutionary phases: 1) seedlings, and 2) saplings/adults. These are based on the phases presented by Clarke (1995). The first three developmental stages of the conceptual approach by Dunlop et al. (2023) that are presented in the model, correspond to the development of the mangrove forest (seedlings and saplings/adults) in response to hydro-morphological change, while the fourth stage refers to the impact that the mangroves have on the surrounding environment. The presence and continued growth of mangroves are governed by the timing and duration of climate forcing that the mangroves can withstand. These influential parameters in combination with the complex dynamics across the lifecycle drive mangrove development and are the theoretical underpinnings of the LEAF (v.1.0) model. To investigate the relative influence of core input parameters on model outcomes, detailed sensitivity analyses were conducted (see Section 2.6).

Within each developmental stage of the model, user input parameters and relationships are required to tailor the model to the project site and mangrove species. In LEAF (v.1.0), these inputs have been collated from academic literature and field measurements for *Avicennia marina*. Data at the species level have been adopted in lieu of site-specific data, which would provide greater accuracy for the model. Where limited data is available for *Avicennia marina*, inputs were based on other *Avicennia* sp. or from global mangrove studies. These inputs, the formulas used throughout the model, and the associated mangrove species are presented and referenced in Appendix A. Further details on how these formulas are incorporated into the model can be found in the source code. Model inputs that are independent of mangrove species or are specific to the site are similarly referenced. The physical parameters assessed for each developmental stage are presented with diagrams and notation in Fig. 2. The logical processes discussed herein refer to those present in LEAF (v.1.0), with flow chart diagrams outlining the decision trees for these processes presented in Appendix B.

2.2.2. Establishment

The establishment stage of the model refers to the calculation of environmental conditions suitable for the recruitment and colonisation of mangroves on the shoreline. If mature mangroves already exist on-site, the model checks whether the grid cells available for establishment are within the user-defined fruiting/seeding window and within an appropriate distance from the mature trees for seed dispersal. If these conditions are met, then the hydrodynamic conditions required for establishment are evaluated.

For *Avicennia marina*, and mangroves generally, these conditions are based on three Windows of Opportunity (Balke et al., 2011) and inform whether a seedling establishes. The first window is evaluated to determine if there is a sufficiently long inundation-free period for the propagule to settle and begin growing roots. A user-defined percentage chance of establishment is applied to this first window to enact natural variability within the model and limit the overestimation of seedling density. This is included to encapsulate the impacts of small-scale disturbances that are outside the scope of hydrodynamic modelling, such as the impacts of light, nutrient, and competition, that might hinder the evolutionary process of the mangroves. Once the propagule has settled and begins to grow roots, a second window of opportunity is evaluated to determine if the bed shear stress is greater than the critical bed shear stress required to dislodge the propagule. If the propagule root length is sufficient to resist this stress, then the shoot will grow. The critical erosion limit is then calculated based on the shoot length. If the change in bed level is below this limit, the third window is fulfilled, and the seedling will successfully establish. An illustration of the establishment logic, and the key input parameters with respect to *Avicennia marina*, are presented in Fig. 2a.

2.2.3. Growth

Modelling mangrove growth is critical to understanding when the forest can become self-sustaining under changing conditions. The magnitude and speed of the growth is dependent on the health of the mangroves and the impacting environmental and hydro-morphodynamic conditions. With sufficient long-term field data, it is expected that relationships can be derived between growth and these

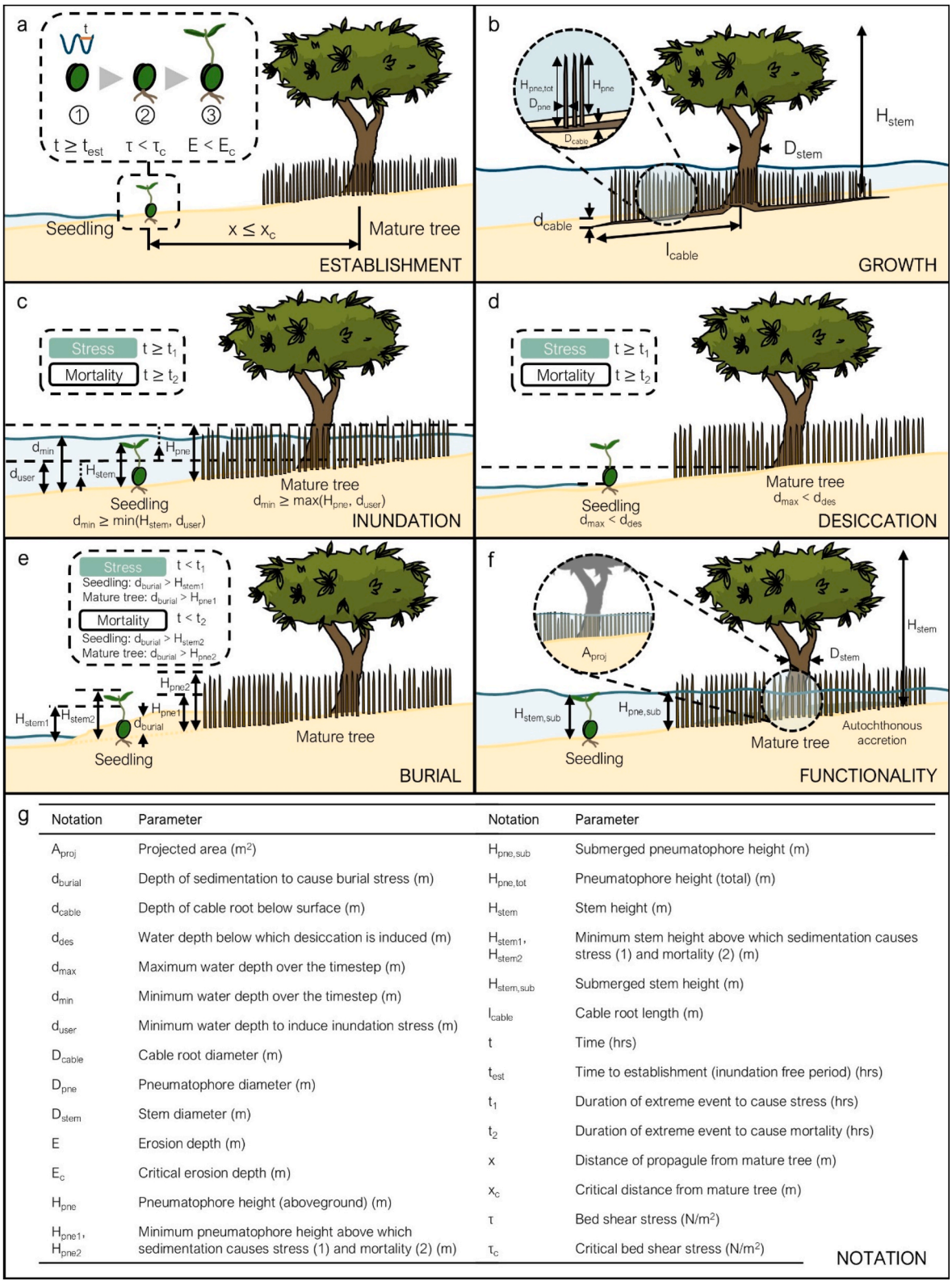

g

Notation	Parameter	Notation	Parameter
A_{proj}	Projected area (m^2)	$H_{pne,sub}$	Submerged pneumatophore height (m)
d_{burial}	Depth of sedimentation to cause burial stress (m)	$H_{pne,tot}$	Pneumatophore height (total) (m)
d_{cable}	Depth of cable root below surface (m)	H_{stem}	Stem height (m)
d_{des}	Water depth below which desiccation is induced (m)	H_{stem1}, H_{stem2}	Minimum stem height above which sedimentation causes stress (1) and mortality (2) (m)
d_{max}	Maximum water depth over the timestep (m)	$H_{stem,sub}$	Submerged stem height (m)
d_{min}	Minimum water depth over the timestep (m)	l_{cable}	Cable root length (m)
d_{user}	Minimum water depth to induce inundation stress (m)	t	Time (hrs)
D_{cable}	Cable root diameter (m)	t_{est}	Time to establishment (inundation free period) (hrs)
D_{pne}	Pneumatophore diameter (m)	t_1	Duration of extreme event to cause stress (hrs)
D_{stem}	Stem diameter (m)	t_2	Duration of extreme event to cause mortality (hrs)
E	Erosion depth (m)	x	Distance of propagule from mature tree (m)
E_c	Critical erosion depth (m)	x_c	Critical distance from mature tree (m)
H_{pne}	Pneumatophore height (aboveground) (m)	τ	Bed shear stress (N/m^2)
H_{pne1}, H_{pne2}	Minimum pneumatophore height above which sedimentation causes stress (1) and mortality (2) (m)	τ_c	Critical bed shear stress (N/m^2)

NOTATION

Fig. 2. Diagrams and notation of the logic for the key stages of the LEAF (v.1.0) mangrove model. (a) Establishment stage with three windows of opportunity; (b) Growth stage identifying key physical attributes; (c) Inundation logic; (d) Desiccation logic; (e) Burial logic; (f) Functional parameters that are returned to the hydromorphodynamic model; (g) Parameter notation.

conditions (Dunlop et al., 2023). However, many relationships have not yet been derived nor made available in academic research, and, as a result, educated assumptions are frequently used in ecosystem modelling. As such, LEAF (v.1.0) incorporates combinations of detailed relationships and simplified assumptions for the growth of *Avicennia marina*.

LEAF (v.1.0) includes the growth for the seedling phase, where early shoot and root development takes place, and the sapling/adult phase,

where growth is based on research for more mature forests. Distinctions between growth phases (e.g., via age or stem height (Clarke, 1995)) are incorporated to align with the changing physical characteristics and biological processes of ecosystems as they evolve. For each growth phase, the growth model logic first considers whether individual mangrove stems are recovering from stress, undergoing stress, or have suffered mortality from a range of hydro-morphodynamic conditions. If mangroves are undergoing stress, the growth rate is adjusted based on a linear fitness function (van Oorschot et al., 2016), which determines the degree of stress with respect to the mortality threshold (Fig. 2b). When mangroves are in the recovery stage, a 75 % growth rate is adopted. No growth occurs when mangroves have suffered mortality. This logic is defined by the user and can be replaced with parabolic or sigmoidal relationships as incorporated in the fitness functions of previous mangrove modelling studies (van Maanen et al., 2015; Xie et al., 2020).

For both the seedling and sapling/adult stages, allometric growth relationships connecting cable root length to cable root diameter, stem diameter to stem height, and pneumatophore diameter to pneumatophore height, have been derived in academic research and are included in LEAF (v.1.0). Pneumatophore growth begins once the cable root has reached the required length in accordance with a user-defined interval between pneumatophores, based on density observed in the field. Pneumatophore growth is assumed to continue if the pneumatophore height is below the maximum water level for the timestep. Growth rates are proportionally reduced when inundation, desiccation, or burial stress occurs, but are maintained during periods of inundation and burial stress because of their observed response to these conditions to retrieve oxygen for the stem (van Bijsterveldt et al., 2023). In the seedling phase, shoot growth only begins once a threshold root length is reached (Balke et al., 2015). A visual representation of the parameter logic is presented in Fig. 2b.

2.2.4. Recovery and mortality

Mangrove response and recovery capacity when exposed to environmental pressures are based on the threshold relationships between mangrove size and the magnitude and duration of the environmental conditions. Chronic stressors of sea level rise, prolonged high- and low-water levels, as well as acute hazards of storm surge, sediment deposition, and bed shear stresses caused by waves and currents, have been considered in LEAF (v.1.0). Wind and wave forces that may induce toppling or breaking of mangrove trees, such as those from extreme storm events, have not been included in this version.

The mortality regimes considered in this study are: 1) inundation, 2) desiccation, 3) burial, and 4) senescence. For each of the first three regimes, individual mangroves are assigned a status as one of: i) healthy, where no mortality regimes are impacting the mangrove, ii) recovery, where the mangrove is in a user-defined period of recovery following impacts from an extreme event, iii) stress, where the mangrove is impacted by an extreme event, and iv) mortality, where the magnitude and duration of the extreme event are beyond the lifecycle threshold for the mangrove. For regime 4, mangroves beyond a threshold age are assumed to no longer persist/grow. For all mangroves that have established as seedlings and suffered mortality, the user is given the option to either keep these mangroves in the system (e.g., to contribute to the available biomass), or to remove them from system. A stem height threshold is included such that dead mangroves with heights below this threshold are removed to provide space for new seedlings. In the event of a second extreme event occurring during the period of recovery, the required recovery timeframe is assumed to increase by a user-defined period.

For the inundation mortality regime, stress and mortality are defined when either a user-defined proportion of the stem height (seedlings) or pneumatophores (saplings/adults) is below the minimum water level, or a minimum water depth is achieved, for user-defined durations. Stress and mortality for desiccation similarly rely on a magnitude and duration of water depth. A mangrove is assumed to desiccate when the water depth falls below a user defined threshold (in this case, 0.0001m) for a set period. Diagrammatic explanations of the parameters included within the inundation and desiccation mortality regimes are presented in Fig. 2c and d, respectively.

Sudden sediment deposition, such as via high discharge events following storms, can induce mangrove mortality by covering a proportion of the stem height (seedlings) or a proportion of the above-ground pneumatophore height (saplings/adult trees). It is assumed that there is no recovery under severe burial events, but recruitment of new seedlings is still possible (Paling et al., 2008). This logic is incorporated into the burial mortality regime in LEAF (v.1.0). The parameters included in the burial mortality regime are illustrated in Fig. 2e.

2.2.5. Functionality

The functionality stage in LEAF (v.1.0) refers to the capacity of the mangrove forest to attenuate incident wave energy and flow velocities, reduce shoreline erosion, store carbon in above- and below-ground biomass, and increase bed levels via autochthonous accretion. These outcomes are influenced by the way mangrove morphology is represented by the user in the model, including either vertical rigid cylinders (Suzuki et al., 2012) or the true morphology of trees observed on-site (van Hespen et al., 2023). From the defined mangrove morphology, physical attributes are calculated and exchanged with the DFM model. The modified Baptist bulk roughness formulae for vegetation (Baptist et al., 2007) is activated in the DFM model to apply a bulk roughness value to each grid cell that contains mangroves. These formulae underpin the representation of mangroves within the DFM model and require the calculated vegetation height, diameter, density, bulk drag coefficient, and bare bed resistance at every timestep.

Because drag parameterisation in vegetation modelling can be undertaken in many ways (van Wesenbeeck et al., 2022), LEAF (v.1.0) enables the user to apply their own bulk drag coefficient formulations. In LEAF (v.1.0), the drag coefficient is calculated based on a characteristic length for longitudinal flow velocities, informed by the projected area and volume of all objects beneath the waterline (Mazda et al., 1997; van Maanen et al., 2015). To inform the characteristic length, several equations have been included for the projected area and volume, from calculations for cylindrical stems and conical pneumatophores (Du et al., 2021), to detailed allometric pneumatophore models (Jerez Nova, 2022).

Allometric equations can also be used to evaluate above- and below-ground biomass estimates, which are critical for understanding how carbon storage changes over time. Equations for the biomass of mature *Avicennia marina* (Comley and McGuinness, 2005) and *Avicennia alba* (Komiyama et al., 2005) have been included as model output options for the user. Similarly, the user can include a rate of autochthonous accretion based on physical mangrove attributes which can locally increase the bed level every timestep. The key parameters considered for mangrove functionality are presented in Fig. 2f.

2.3. Model setup

The setup of LEAF (v.1.0) requires populating a list of input parameters with values relevant to the species and site being modelled. A summary of the inputs that can be updated in the model input file of LEAF (v.1.0), as well as the inputs and logical expressions that can be updated in the main code file are provided in Table 1. The full list of inputs and the values adopted for the base case model run are presented in Appendix A. Accompanying the model code are guidance notes, which have been developed to provide support for editing and updating the model with new inputs from the user's project site. These notes include the locations within the model code where the user can provide detailed equations and parameter relationships.

Table 1
Summary of the inputs for version 1.0 of the mangrove LEAF model.

Model component	Input file	Main code
1. Time	Timestep duration; number of timesteps, fruiting window	N/A
2. Plotting	Plotting interval	Plotting parameters
3. Initial mangroves	Mangrove presence; density; stem height and diameter; cable root length and diameter; pneumatophore length and diameter; age	N/A
4. Mangrove extrema	Maximum stem density, height and diameter, cable root length and diameter, number of cable roots, and pneumatophore diameter	N/A
5. Other mangrove parameters	Seedling to sapling height threshold; fecundity age; cable root depth; pneumatophore spacing; autochthonous accretion rate; starting cable root length and diameter; starting pneumatophore diameter	Parameter separating seedlings from saplings/ young adults
6. Establishment	Distance at which seeds can settle from fecund trees; inundation free period; chance of establishment; critical bed shear stress; cable root length requirement for shoot growth; critical erosion depth	Additional equations to calculate critical bed shear stress and erosion depth
7. Growth	Growth logic; seedling and sapling/young adult growth parameters for: stem diameter, stem height to diameter relationship, cable root length, cable root diameter to length relationship; pneumatophore growth condition; pneumatophore diameter growth rate; pneumatophore height to diameter relationship	Growth logic; additional allometric relationships
8. Recovery and Mortality	Removal of dead mangroves; stem height threshold for removing dead mangroves	Mangrove health categories; Removal logic
	Proportion of stem height/ pneumatophore length inundated to cause stress and mortality; duration of inundation to cause stress and mortality; recovery duration; additional recovery required due to successive events; maximum number of inundation events; water depth for desiccation	Inundation logic
	Water depth threshold for desiccation; duration of desiccation to cause stress and mortality; recovery duration; additional recovery required due to successive events; maximum number of desiccation events	Desiccation logic
	Maximum number of timesteps over which sedimentation is assumed to be gradual; proportion of stem height/ pneumatophore length buried to cause stress and mortality; duration of burial to cause stress and mortality	Burial logic
	Maximum age	Senescence logic
9. Functionality	Projected area and volume equations for stems and pneumatophores; drag coefficient equation; proportion of stem heights and diameters in each grid cell that are exchanged with hydro-morphodynamic model; above-ground and below-ground biomass equations; autochthonous accretion	Additional equations for projected area, projected volume, drag coefficient, and biomass

2.4. Hydro-morphodynamic model

2.4.1. Model layout

To test LEAF (v.1.0), the model was integrated with a 2D depth-averaged hydro-morphodynamic model in Delft3D Flexible Mesh (DFM) using a schematised nearshore section of an estuarine shoreline (Fig. 3). The rectangular grid comprised 500 square (5 × 5m) grid cells, with total grid dimensions of 250m in the cross-shore direction, and 50m alongshore. This model setup was established with tides and waves normal to the shoreline, mimicking typical hydrodynamic estuarine conditions with irregular wind waves and/or boat wake. A slope of 1V:100H was adopted to enable elevation increments of 0.05m across each grid cell. This simplified setup enabled the modelled mangrove distribution to be validated to within a 0.05m tolerance against measured seaward and landward limits of mangrove forest extents at four sites in NSW (Henderson and Glamore, 2024b). These four sites (Table 2) represented different estuary typologies (Dunlop et al., 2025):

1) Drowned River Valley (DRV), characterised by oceanic tidal conditions regardless of catchment flooding inputs (Hanslow et al., 2018).
2) Large Barrier Estuary (LBE), characterised by narrow or constrained downstream confluences that attenuate tidal wave propagation, with upstream areas of tidal amplification, and short-term flooding (Morris et al., 2013).
3) Small Barrier Estuary (SBE), characterised by tidal dampening at the ocean entrance and an attenuating tidal plane with distance upstream. Overall reduced ability for flood drainage and longer flooding periods (Morris et al., 2013).
4) Intermittently Open and Closed Estuary (IOCE), characterised by an entrance that is semi-permanently open (Kennedy et al., 2020), acting as a barrier estuary when open, and separated from all tidal dynamics when closed. Long periods of flooding/inundation.

2.4.2. Model scenarios

For the schematised shoreline, two scenarios were considered to test the model functionality, validate the mangrove extents against field measurements, and conduct a sensitivity analysis of input parameters:

A. **Restoration site** where mangrove propagules colonise an empty shoreline. This scenario was developed to test model functionality, validation, and for sensitivity testing of input parameters; and
B. **Existing forest** where propagules colonise within proximity to fecund trees (assumed to be trees >1 year old). This scenario was developed to test the functionality of the model to recruit new seedlings from mature mangroves and to examine the response of an existing forest to bed level change.

Scenarios A and B were both used to test the model functionality to produce a range of outputs corresponding to mangrove stem and root size and density, biomass, and coastal protection parameters. Scenario A was run using the continuous historical water level time series data from tide gauges in proximity to each site (Manly Hydraulics Laboratory, 2024), with a morphological factor of one. This enabled outputs to be observed at the morphological conditions as would be expected in the

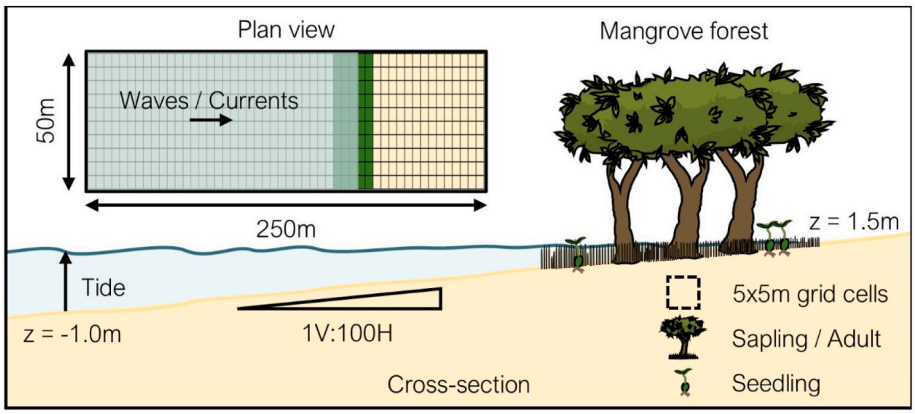

Fig. 3. DFM model setup with schematised nearshore section of an estuarine shoreline and hydrodynamic boundary conditions.

Table 2
Measured mangrove extents and historical water level data for the four estuary sites.

Estuary typology	Site	Measured mangrove forest extent (mAHD[a]) Henderson and Glamore (2024b)		Continuous water level time series (Manly Hydraulics Laboratory, 2024)	
		Seaward	Landward	Duration (years)	Timeframe
DRV	1.Spencer, Hawkesbury River	0.17	0.79	7	January 15, 2017–January 15, 2024
LBE	2. Minnamurra, Minnamurra River	0.06	0.68	5	January 15, 2019–January 15, 2024
SBE	3. Farquhar Inlet, Manning River	0.14	0.54	12	January 15, 2012–January 15, 2024
IOCE	4. Gerroa, Crooked River	0.41	0.73	6	May 08, 2013–May 08, 2019

[a] Elevations recorded in metres relative to the Australian Height Datum (mAHD).

field. A linear bed profile comprising sandy sediment was adopted with a reference settling density of 1600 kg/m^3 and a specific density of 2650 kg/m^3 in line with the values adopted in previous ecosystem modelling studies (Beselly et al., 2023; Best et al., 2018; Dzimballa et al., 2025; Gijsman et al., 2024a).

Both scenarios were run for one year, where D-Flow was coupled with D-Waves. Wave conditions were introduced in these model runs to change the bed level. Constant wave conditions were applied within the model, with a significant wave height of 0.1m and a period of 3s at the offshore boundary. A morphological factor of 10 was applied with the wave model to enhance the bed level change. This increased rate of bed level change impacted the establishment processes of mangroves because it created increased erosion or accretion that otherwise would not occur over the approximate 12hr timeframes required for establishment (see Section 2.2.2). For simplicity, it was assumed that the mangrove stems and pneumatophores occupied the same bed elevation within each grid cell. This second set of model runs was conducted for a linear bed profile comprising sand, an equilibrium bed profile comprising sand (following a one-year model run without mangroves), and a linear bed profile comprising mud. For the mud profile, a dry bed density of 500 kg/m^3 was adopted.

In both scenarios, a time interval of 12s was chosen for updating the water levels. This interval is in the order of the intervals (6–30s) adopted in other biophysical modelling studies (Best et al., 2018; Brückner et al., 2019; Willemsen et al., 2022). A time interval of 1day was adopted for relaying the wave computations from D-Waves to the D-Flow module. A larger communication time interval reduced the computational effort required to run the coupled D-Waves and D-Flow model. LEAF (v.1.0) was coupled with the DFM model every 12hrs. The impact of adjusting the mangrove timestep was assessed in the sensitivity analysis (see Section 2.6.2).

Validation of the mangrove extents and the sensitivity analysis were only carried out for Scenario A to avoid the inclusion of any biases associated with an existing mangrove forest (e.g., in Scenario B). Model durations matched the length of the available continuous water level time series for the site, and a morphological factor of 1 was adopted.

2.5. Model validation

Typically, inputs and logical expressions within LEAF (v.1.0) were taken from peer-reviewed research as documented in the model code and associated guidance notes. However, due to the complexity of modelling mangroves, many conditions related to the long-term biophysical processes have not yet been researched, and some aspects of the model rely on assumptions. It is therefore important to independently validate the LEAF model as rigorously as possible.

To this aim, the calculation processes for each parameter in LEAF (v.1.0) have been systematically tested by qualitatively observing the change in mangrove development or bed level changes over time. This process testing was carried out using short model runs on a simplified grid during model development.

Secondly, the model outcomes were also validated, using mangrove distributions across different estuary typologies. The modelled spatial extent of the mangrove forest in Scenario A was compared with field measurements of the seaward and landward elevation limits of four sites presented in Table 2. The longest continuous water level time series obtained from tide gauge records at each site (Manly Hydraulics Laboratory, 2024) were used as boundary conditions in the model. These time series presented water elevations typically every 15mins, and the series was deemed continuous if the time between consecutive recordings were less than 3hrs. The modelled seaward and landward elevations of the resultant cross-shore distribution (i.e., grid cells occupied by living mangroves) were compared to the elevation limits of mangrove extent as measured by Henderson and Glamore (2024b). Where initial model runs did not result in close alignment, input parameters associated with the mortality regimes of inundation and desiccation were adjusted to achieve validation for the estuary. These parameters were recorded and compared for each estuary typology (see Section 3.2).

2.6. Sensitivity analysis

In addition to the LEAF (v.1.0) model validation, sensitivity analyses were undertaken for Scenario A to identify the sensitivity of the model

outputs, such as mangrove size and extent, to: (i) model duration, (ii) mangrove timestep and (iii) mangrove input parameters.

The model duration and water level time series for the four study sites (Table 2) were varied to identify the required model duration for the convergence of mangrove establishment and mortality zones, as well as the overall seaward and landward extents for each estuary typology. The aim of this analysis was to identify the minimum time needed to model mangrove extents, to reduce computational effort.

The mangrove timestep was varied at Site 1 (Spencer, Hawkesbury River (DRV)) to examine the impact on the mangrove extent. As statistical variables, such as maximum water depth, are used in LEAF (v.1.0), shorter timesteps may provide more discrete results. To establish the minimum required time step, the elevation gradient at which mangroves established was observed and compared for timesteps of 24hrs, 12hrs, 6hrs, and 3hrs.

To assess the sensitivity of LEAF (v.1.0) to the large number of input parameters, detailed sensitivities were assessed for Site 1 (Spencer, Hawkesbury River (DRV)), and Site 4 (Gerroa, Crooked River (IOCE)). These two sites represented estuary typologies that either have consistent forcing conditions (DRV) or that experience long periods of extreme water level changes (IOCE).

A base case model was established for each mangrove site using the available continuous water level time series. The base case results were compared to the results of the sensitivity model scenarios, where unique parameters were varied. A list of all sensitivity tests is presented in Appendix C. The range of values tested for each parameter was based on field and laboratory data presented in peer-reviewed literature. Input parameters with the greatest influence on mangrove forest development are recommended for inclusion within future modelling efforts.

3. Results

3.1. Model functionality

3.1.1. Model outputs

LEAF (v.1.0) has been developed such that the variables associated with mangrove forest development, mortality regimes, and environmental forcing are exported and observed at user-defined time intervals. At each time interval, the vertical cross-sectional profile of the shoreline can be observed (Fig. 4a). When the spatial extent of the forest changes, the user can observe the grid cells impacted by mortality regimes of inundation, desiccation, and burial (Fig. 4b). Outputs corresponding to mangrove presence, stem and root height, diameter, and density, enable the user to visually and quantitatively track the growth and change in mangrove forest size and spatial extent (see examples of stem and pneumatophore density in Fig. 4c-d). The variables that influence the change in growth and the mortality of the forest, such as bed level, bed shear stress, and water depth, are also recorded to provide causes of

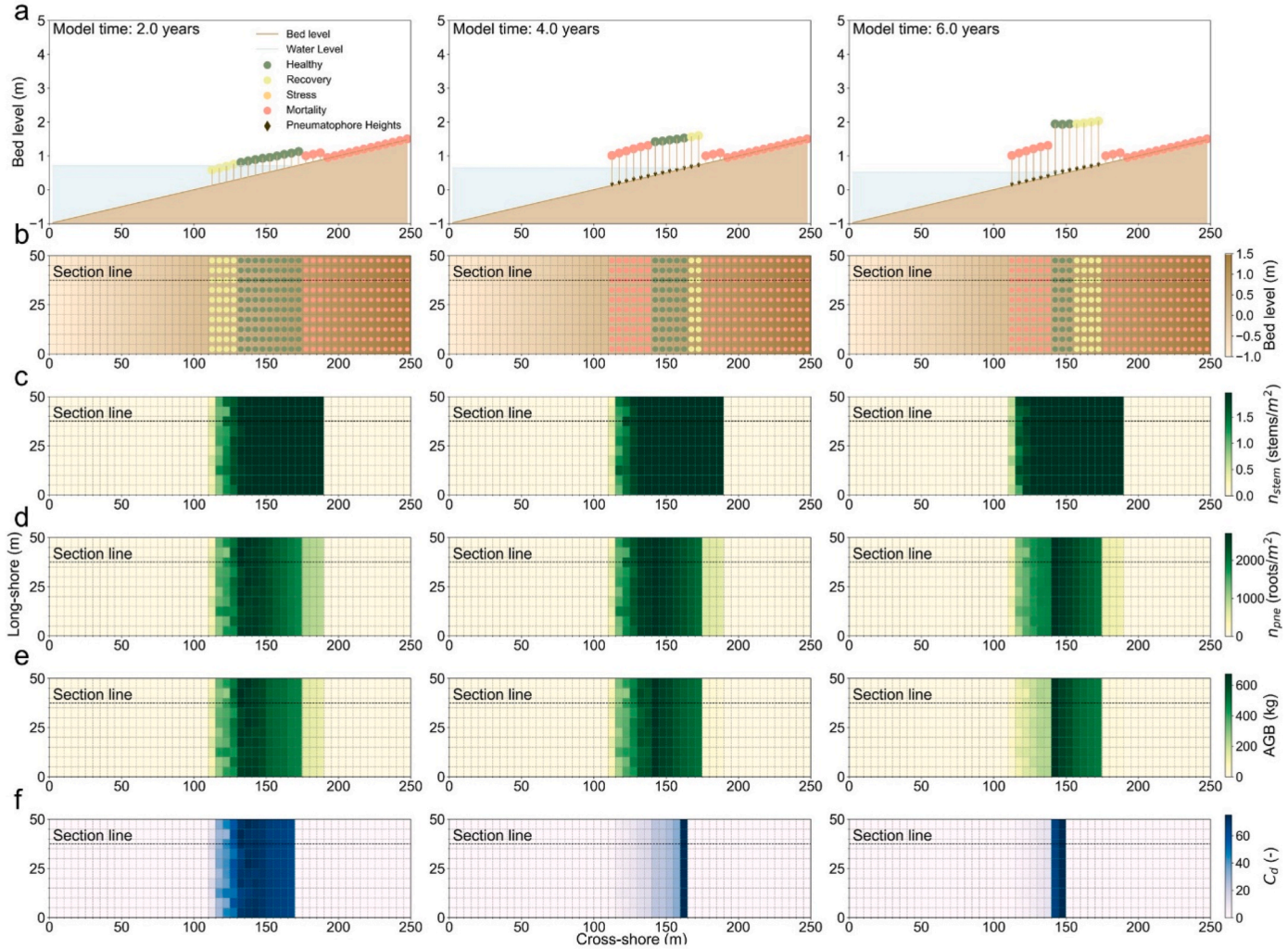

Fig. 4. Example LEAF (v.1.0) outputs from the base case run at Site 4 (Gerroa, Crooked River (IOCE)) at 2-year intervals. (a) Cross-section of mangrove extent and health; (b) Plan-view of mangrove extent and health; (c) Stem density (stems/m^2); (d) Pneumatophore density (pneumatophores/m^2); (e) Above-ground biomass (kg); (f) Drag coefficient (−).

predicted mangrove forest dynamics. Finally, variables linked to the ecosystem services of carbon sequestration, such as above-ground biomass (Fig. 4e) and below-ground biomass, and coastal protection, such as projected area, volume, and drag coefficient (Fig. 4f), are also exported for each grid cell in the model. These outputs present an example of how LEAF (v.1.0) can be used to predict and compare the performance of mangrove forests throughout their lifecycle. Plotting and exporting the data stored in each variable enables the user to track the temporal dynamics of the mangrove forest (see **Video 1)**.

Videos related to this article can be found online at https://doi.org/10.1016/j.envsoft.2025.106619.

Video 1 Mangrove development over time at Site 4 (Gerroa, Crooked River (IOCE)).

3.1.2. *Morphological change*

Under waves and high flows, a shoreline may experience high bed shear stresses that move sediment to cause accretion and erosion (Fig. 5). These processes impact the establishment of mangroves in LEAF (v.1.0), where seedlings may colonise new parts of the shoreline because of the higher elevations offered by the accreted nearshore profile. The size and density of the mangrove forest inform the drag and roughness coefficients. Changes to the morphology of the shoreline during mangrove restoration are shown for both Scenario A and B at Site 1 (Spencer, Hawkesbury River (DRV)) in **Video 2** and **Video 3,** respectively.

Videos related to this article can be found online at https://doi.org/10.1016/j.envsoft.2025.106619.

LEAF (v.1.0) also includes the interaction between sediment and mangroves, which are critical for understanding relevant processes for mangrove development. Model functionality includes the capacity for seedlings to be buried or dislodged and for the burial of pneumatophores to cause mangrove mortality when pneumatophore growth is unable to reach the surface level within a user-defined timeframe. Changes in roughness and drag are also important as they influence the sediment deposition through the forest.

Video 2 The temporal dynamics of the mangrove forest in Scenario A at Site 1 (Spencer, Hawkesbury River (DRV)) for model run i).

Video 3 The temporal dynamics of the mangrove forest in Scenario B at Site 1 (Spencer, Hawkesbury River (DRV)) for model run i).

3.2. *Model validation*

As outlined in Section 2.5, LEAF (v.1.0) was validated with mangrove observations from four field sites. In this section, the comparative analysis is presented, highlighting the performance of the LEAF (v.1.0) model to accurately replicate mangrove forest extent. The outcomes of the validation modelling are presented in Fig. 6 and Table 3.

3.2.1. *Drowned river valley*

For Site 1 (Spencer, Hawkesbury River (DRV)), validation of the

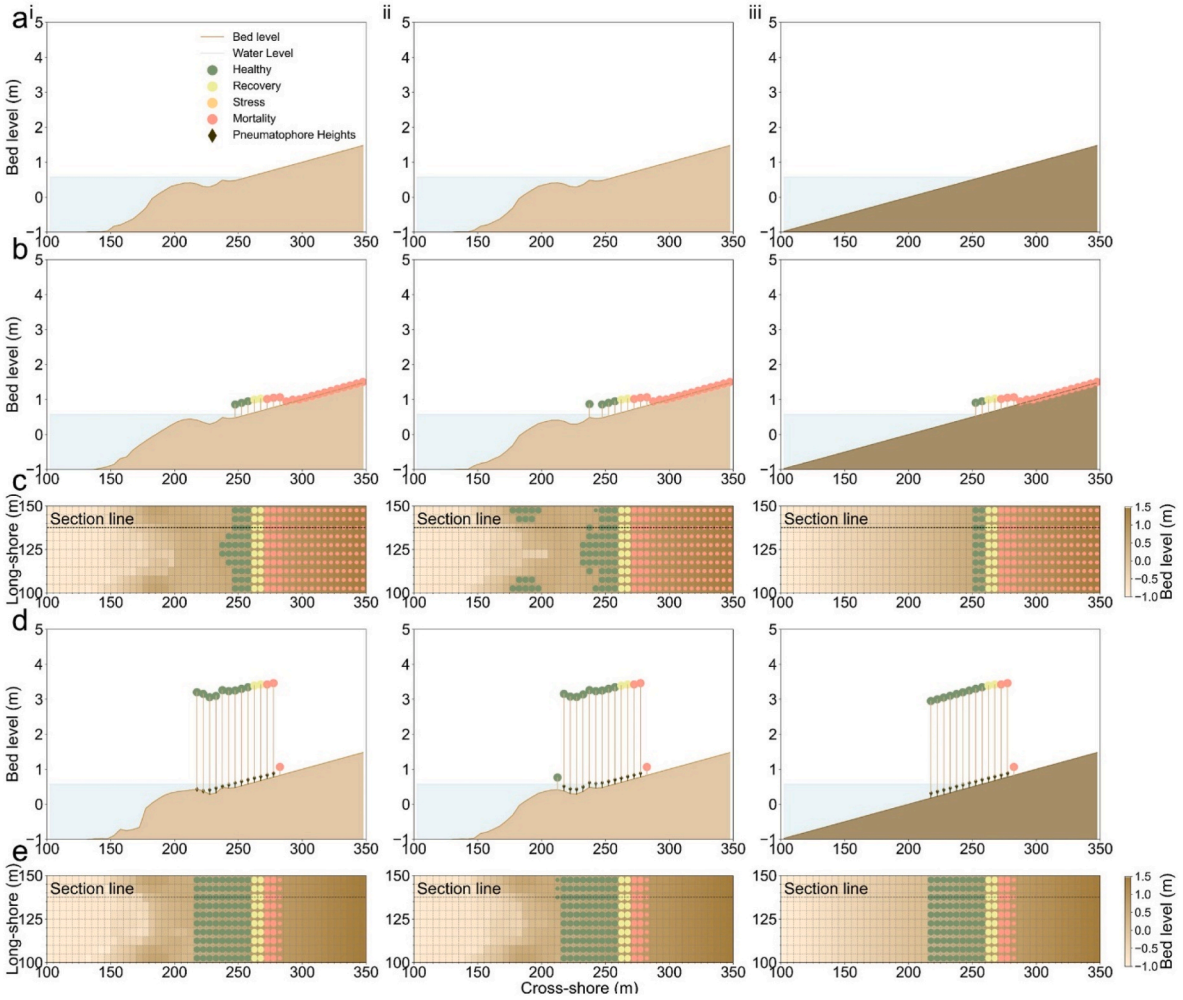

Fig. 5. The response of mangrove growth to morphological change at Site 1 (Spencer, Hawkesbury River (DRV)) for model runs with i) a sandy shoreline with an initial linear profile; ii) a sandy shoreline with an initial equilibrium profile; and iii) a muddy shoreline with an initial linear profile. Model runs include a) no mangroves, b) Scenario A - an infinite abundance of seeds, c) plan view of b); d) Scenario B - an existing forest, e) plan view of d).

landward extent was achieved by varying the duration at which mortality from desiccation was induced for both seedlings and saplings (Fig. 6a). A duration of between 24 and 43 days yielded mangroves persisting at an elevation between 0.775 and 0.825mAHD, closest to the measured elevation in the field of 0.79mAHD, given the 0.05m increments in the model grid cell setup. The upper limit of this duration, 43 days, resulted in the widest extent of healthy mangroves, while the lower limit, 24 days, resulted in the greatest proportion of the mangrove distribution under periodic stress from desiccation, but without mortality. For the seaward extent, no stress or mortality from inundation was observed over the 7-year validation period. Inundation was not observed because the base case inputs for the establishment stage, notably the inundation free period, did not permit the colonisation of mangrove propagules at lower elevations. The lowest elevation at which mangroves established in the model, 0.175mAHD aligned with the seaward extent measured in the field, 0.17mAHD (Fig. 6a).

3.2.2. Large Barrier Estuary

Validation was similarly achieved at Site 2 (Minnamurra, Minnamurra River (LBE)), by altering the parameters associated with the magnitude and duration of desiccation (Fig. 6b). The duration of desiccation was observed to lie between days for Site 2 to achieve an elevation at the landward extent of 0.675–0.725mAHD, aligning with the 0.68mAHD measured in the field. A similar proportion of the mangrove extent was observed to be under stress at the lower limit of the duration (14 days). Like Site 1, no prolonged inundation was observed at Site 2 over the validation period, in this case 5 years, and therefore the seaward extent was constrained to the elevations at which mangroves colonised the shoreline. The seaward elevation predicted by the model, 0.125mAHD, did not match the 0.06mAHD measured in the field, with one grid cell difference (Fig. 6b). This was likely caused by the limited continuous water level data at the site. Longer historical time series may have included lower water levels, prior to the constructed entrance changes to the Minnamurra River estuary, permitting the establishment of mangroves at lower elevations. The inundation free period, which influences the elevation at which mangrove establish, was not adjusted during the validation process at any of the sites, because the mangrove timestep was set to 12hrs. Shorter inundation free periods would permit the establishment at lower elevations, but 12hrs (approximately one tidal cycle) best represents the time for *Avicennia marina* establishment in NSW estuaries (Henderson and Glamore, 2024b).

3.2.3. Small Barrier Estuary

At Site 3 (Farquhar Inlet, Manning River (SBE)), the mangrove forest experienced both inundation and desiccation over the 12-year period. For the landward extent, the duration of desiccation causing mangrove mortality, was observed between 26.5 and 54.5days. This range of values resulted in a predicted landward extent of 0.525–0.575mAHD, within the 0.05m tolerance to the measured 0.54mAHD (Fig. 6c). At the seaward edge, elevations of 0.125–0.175mAHD (within the 0.05m tolerance to the measured 0.14mAHD) were only achieved when the inundation depth required to induce mangrove mortality was increased from the base case depth of 0.5m, as measured by Henderson and Glamore (2024b). As such, water depths of 0.6–0.8m were tested in combination with inundation duration (3.5–11days) to validate the seaward extent at this site. For all permutations that resulted in validation of the mangrove distribution, stress from either inundation or desiccation was observed.

Table 3
Summary of input parameter ranges required to achieve validation of the modelled mangrove extent with field observations of Henderson and Glamore (2024b).

Estuary Typology	Site	Inundation		Desiccation
		Depth (m)	Duration (days)	Duration (days)
DRV	1. Spencer, Hawkesbury River	0.5 (base)	10 (base)	24–43
LBE	2. Minnamurra, Minnamurra River	0.5 (base)	10 (base)	14–25.5
SBE	3. Farquhar Inlet, Manning River	0.6–0.8[a]	3.5–11	26.5–54.5
IOCE	4. Gerroa, Crooked River	0.5 (base)	14–44.5	27–51

[a] Depths greater than the base case value were tested because the base case value did not result in validation of the seaward extent at this site. Depths of 0.6–0.8m were tested and achieved validation.

3.2.4. Intermittently Open and Closed Estuary

The mangrove forest at Site 4 (Gerroa, Crooked River (IOCE)) was similarly exposed to inundation and desiccation over the 6-year validation run, due to long periods of high and low water levels associated with the periodic closure of the entrance to the estuary. The landward extent was validated by adjusting the desiccation duration for mortality to 27–51days. This range predicted an elevation of 0.725–0.775mAHD, aligning with the measured 0.73mAHD (Fig. 6d). The seaward extent was similarly validated by altering the inundation duration for mortality to 14–44.5days. This high tolerance to inundation compared to the other estuary typologies may be explained in the field by Site 4 having

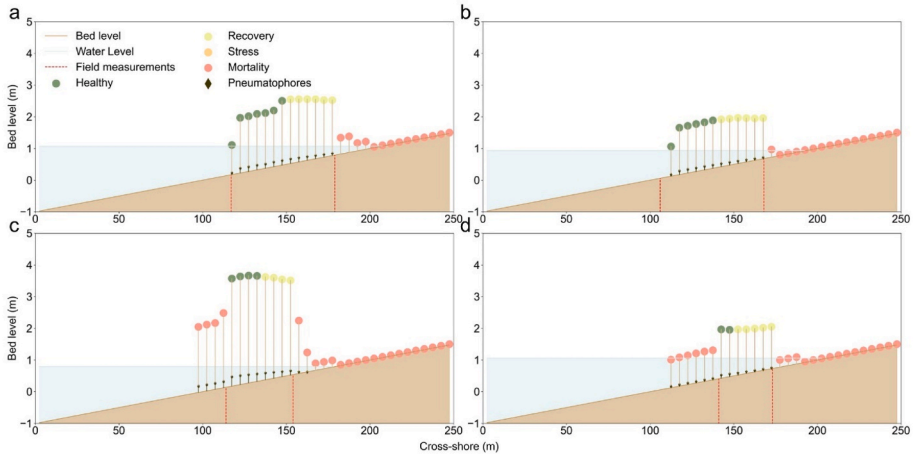

Fig. 6. Comparison of the cross-shore mangrove extents at the end of the model run with the field site observations (dashed red lines) of Henderson and Glamore (2024b): (a) Site 1 (Spencer, Hawkesbury River (DRV)); (b) Site 2 (Minnamurra, Minnamurra River (LBE)); (c) Site 3 (Farquhar Inlet, Manning River (SBE)); (d) Site 4 (Gerroa, Crooked River (IOCE)).

repeated exposure to long periods of flooding, resulting in more resilient mangroves. Further, higher water depths at Site 4 are unlikely to bring larger waves and flows due to the sheltered nature of the IOCE, unlike the other estuary typologies. Using the validated parameters, an elevation of 0.375–0.425mAHD was predicted, aligning with the measured 0.41m, within the 0.05m tolerance of the model setup. The base case inundation depth to induce mangrove mortality (0.5m) resulted in validated seaward extents for this estuary, and therefore no tests at higher inundation depths were conducted. For all adjusted parameters resulting in validation of the mangrove distribution at Site 4, the mangrove forest experienced stress from either inundation or desiccation.

3.3. Sensitivity analysis

In addition to the LEAF (v.1.0) model validation, it is important to understand the sensitivity of the model to the input parameters, such as model duration, mangrove timestep, and mangrove input parameters. A detailed sensitivity analysis of all parameters was conducted with the key results presented in this section and further outcomes in the Supplementary Material.

3.3.1. Model duration

Results from varying the model duration demonstrate that the extent of mangrove presence is less consistent for shorter model durations (Fig. 7). Shorter durations presented a wider range of extents due to fewer fruiting windows and the persistence of water level anomalies caused by floods and droughts for a larger proportion of the model duration. When the model duration and subsequent water level time series are increased, water level anomalies occupy a smaller portion of the timeframe and average conditions persist for most of the model run. This is observed most clearly for the DRV (Fig. 7a) and LBE (Fig. 7b). For the SBE (Fig. 7c) and IOCE (Fig. 7d), the results are more varied and are dependent on the timing of entrance changes in the estuary.

Similarly, by changing the model duration, the mangrove establishment and mortality zones were seen to shift. An example is presented in Fig. 8 at Site 3 (Farquhar Inlet, Manning River (SBE)), indicating that the elevations where mangroves live are different from the rigid limits of mean water level and the mean high-water mark. This supports the notion proposed by Henderson and Glamore (2024b), where an extreme event of flooding or drought can change water levels suddenly and cause mangroves to establish and grow at different elevations. For example, a period with consecutive low water levels between the 5.5- and 6-year marks in Fig. 8a causes desiccation of mangroves and reduces the healthy mangrove extent. If the model runs do not capture this event, the establishment and healthy mangrove zone is likely overpredicted (Fig. 8d). Contrastingly, if the shorter model run has consistent elevated water levels, the seaward mangrove extent is likely underpredicted (Fig. 8b and g). The results similarly shift according to extreme events across the four tested sites (see Figs. S1–S3 in the Supplementary Material).

3.3.2. Mangrove timestep

The timestep for the LEAF model influences the value of the parameters that are retrieved via the BMI interface from the DFM model. A longer timestep means that hydrodynamic parameters are calculated more often within the timestep, giving a larger dataset of parameters from which statistical variables such as minimum and maximum water depth are calculated. The impact of using a larger dataset is shown in Fig. 9 for Site 1 (Spencer, Hawkesbury River (DRV)), where the resultant healthy mangrove extent for a timestep of 24hrs (Fig. 9a) is larger than the extent for smaller timesteps (Fig. 9b–d). This is caused by the distribution of hydrodynamic parameters within the timestep containing lower minimum water levels, meaning that mangroves growing seaward are less impacted by inundation. However, because mangroves have been observed to establish between the peak water levels within tidal cycles (approximately 12hrs) (Henderson and Glamore, 2024b), timesteps of less than 24hrs are more realistic for mangrove establishment.

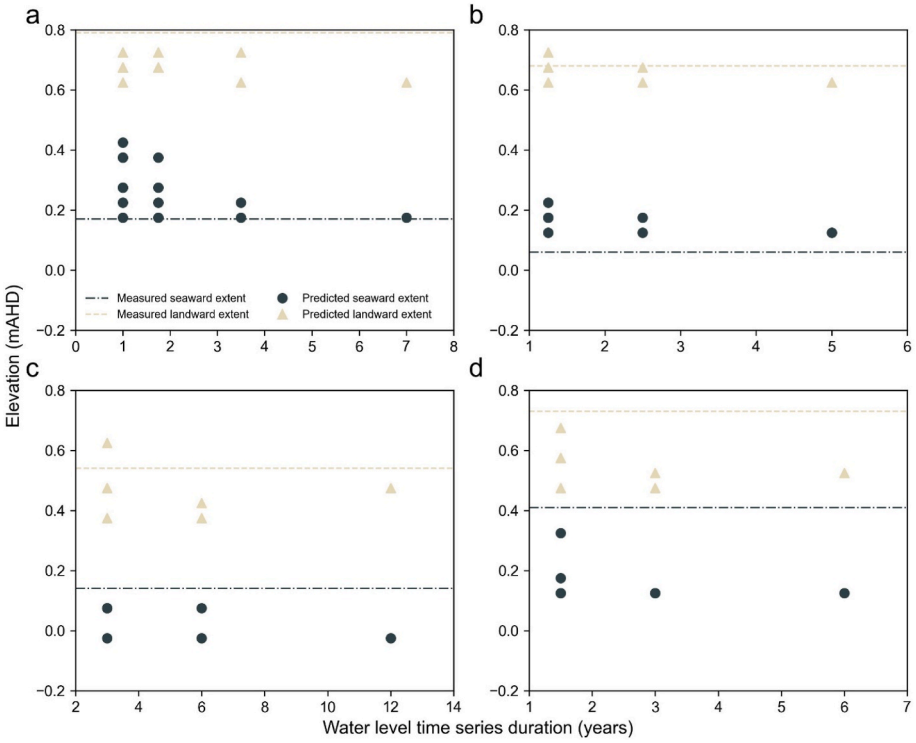

Fig. 7. Sensitivity of seaward and landward mangrove extents for different model durations (dots), compared to field data from Henderson and Glamore (2024b) (dashed lines): (a) Site 1 (Spencer, Hawkesbury River (DRV)); (b) Site 2 (Minnamurra, Minnamurra River (LBE)); (c) Site 3 (Farquhar Inlet, Manning River (SBE)); (d) Site 4 (Gerroa, Crooked River (IOCE)).

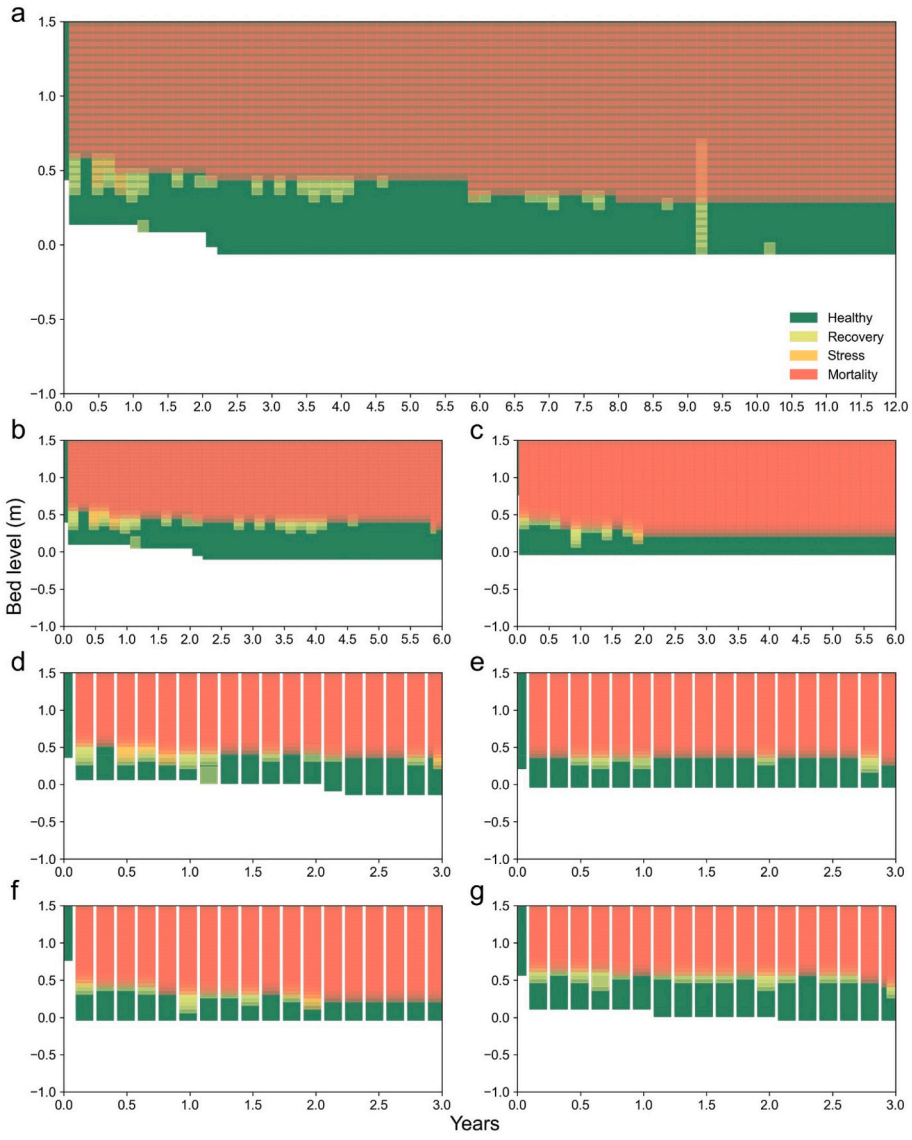

Fig. 8. Plan view of the establishment and mortality zones of mangroves modelled for the base case inputs at Site 3 (Farquhar Inlet, Manning River (SBE)) for a given transect. Zones are shown for model durations of: (a) 12yrs; (b–c) 6yrs; (d–g) 3yrs. Note that the impacts of inundation were not observed for the base case model runs at Site 3.

For timesteps of 12hrs or less, negligible change was observed between the resultant mangrove extent. This indicates that a 12hr timestep, which is more computationally efficient than timesteps of 6hrs or 3hrs, is suitable for modelling mangroves in these estuaries.

3.3.3. *Mangrove parameters*

A detailed sensitivity analysis was conducted to evaluate the sensitivity of mangrove attributes such as size and density, and mangrove zones, to the range of input parameters included within LEAF (v.1.0). Individual results from this analysis are presented in **Supplementary Notes 1** and **2**. The key findings from this analysis are presented in Fig. 10. Reference is made to input parameters that are most critical to long-term modelling, and which researchers should target for inclusion in future models.

Stem height and diameter are sensitive to a wider range of the tested parameters at Site 4 (Gerroa, Crooked River (IOCE)) than at Site 1 (Spencer, Hawkesbury River (DRV)) (Fig. 10a). This is due to the prolonged exposure of the mangrove forest to inundation and desiccation in the IOCE, where the establishment of mangroves occurs at varied elevations, resulting in greater sensitivity of mangrove size at later years in the model run to the tested parameters. The influential parameters from the establishment stage, particularly the fruiting window duration and timing, and the inundation free period, have been documented in peer-reviewed literature and are available for future long-term modelling.

The impact of inundation causes the parameters affecting pneumatophore growth to have greater influence on the resultant mangrove stem size, in response to the pneumatophores bio-adapting to survive inundation pressures (Toma et al., 1991). Similarly, parameters associated with the depth and duration of inundation that cause mangrove mortality are more influential at Site 4 than at Site 1. These parameters, which directly affect the mortality of mangroves, have not been researched extensively and further research is recommended in this field. Like the stems, pneumatophore diameter and height are more sensitive to the parameters from the establishment stage and inundation mortality regime at Site 4 than at Site 1 (Fig. 10b). However, model sensitivity is lower for pneumatophores than for stems, because pneumatophores can maintain and increase growth during periods of stress (Okello et al., 2020). Differences between the sensitivity of stem and pneumatophore density to the tested parameters is negligible between the sites. Limited change was also observed for the mangrove zonation,

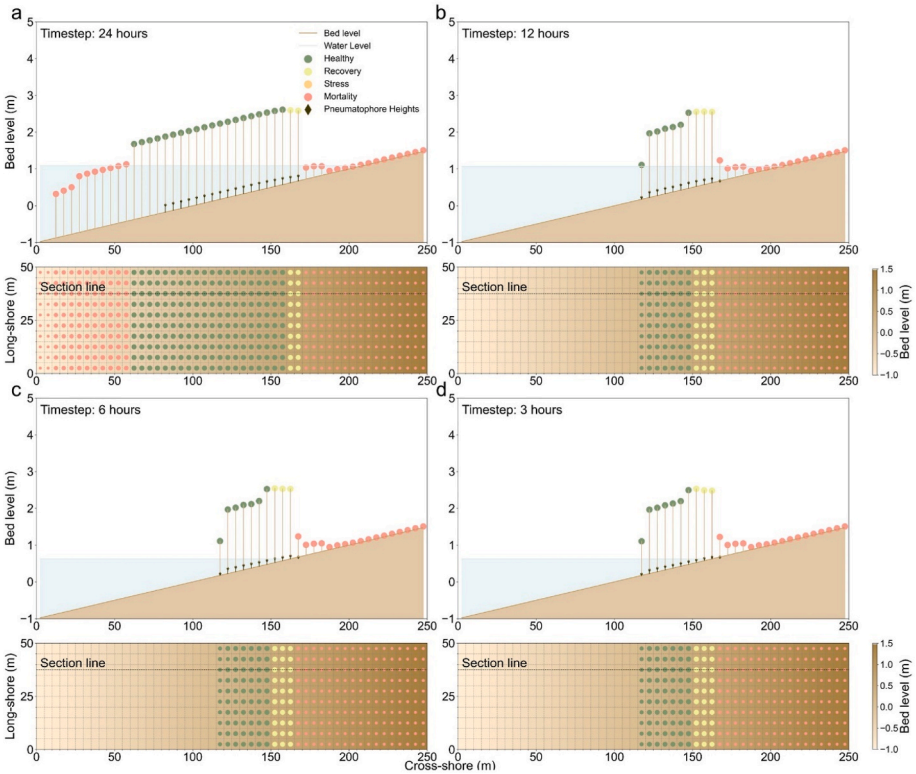

Fig. 9. Comparison of mangrove establishment zones and stem density results at Site 1 (Spencer, Hawkesbury River (DRV)) for different mangrove timesteps: (a) 24hrs; (b) 12hrs; (c) 6hrs; (d) 3hrs.

with the healthy mangrove and inundation zones influenced by more parameters at Site 4 due to the tidal hydrodynamics and resultant inundation patterns of the site (Fig. 10c). However, this had no discernible impact on the sensitivity of the desiccation zone.

4. Discussion

An individual-based mangrove lifecycle model, LEAF (v.1.0), was developed and tested to simulate the growth, stress, and death of an *Avicennia marina* mangrove forest under multiple biophysical thresholds. Based on local tidal, water level, and climatic forcing conditions, the model predicts the growth and biomass of mangroves across a foreshore. For the first time, the LEAF (v.1.0) model simulates the outputs of mangrove health (i.e., whether or not a mangrove is stressed or has died from hydro-morphodynamic forces), the elevation range of living mangroves, biomass, drag coefficients, projected forested areas and volumes, and a range of growth dependent variables (e.g., stem and pneumatophore density, diameter and height) across the entire mangrove lifecycle. LEAF (v.1.0) successfully predicted the spatial mangrove forest extent across four estuary typologies, each with unique long-term water level datasets characterised by estuarine dynamics. Long-term growth of a mangrove forest was calculated in response to local tide conditions, water level anomalies, sediment deposition, and bed shear stress impacts caused by mild wave conditions. Detailed sensitivity modelling highlighted the linkages between environmental variables and biophysical parameters. The discussion below outlines how the model can be applied to guide mangrove restoration and conservation, inform climate change analyses and support future research.

4.1. Restoration and conservation guidance

The LEAF (v.1.0) model successfully predicted the cross-shore distribution of *Avicennia marina* mangrove forests in four unique estuary typologies. This was achieved by adjusting the critical parameters associated with shoreline inundation and desiccation magnitude and duration within the model. For each validated mangrove forest, the local inundation pattern and desiccation rates were shown to influence the mangrove growth/decay behaviour. For example, the predicted seaward extent of the mangrove forest at Site 3 (Farquhar Inlet, Manning River (SBE)) shifted at irregular intervals due to the dynamic tidal and flooding conditions within the estuary. These temporal changes in the cross-shore distribution of the mangrove forest provide an insight into the drivers of mangrove establishment and survivability, highlighting the different role of chronic (e.g., tidal) stressors versus acute (e.g., flooding and sudden sediment deposition) stressors on mangrove survivability. By evaluating the mangrove lifecycle over longer model durations, the development of the forest in response to these stressors, and the long-term convergence of the mangrove distribution, can be observed. These outputs from LEAF (v.1.0) can be used to quantify the long-term suitability of *Avicennia marina* mangroves on estuarine shorelines across biogeographic regions to compare the viability of different restoration strategies for mangrove species with pencil or cone shaped roots (e.g., *Avicennia* sp., *Laguncularia* sp., and *Sonneratia* sp).

Conservation strategies can similarly be guided by the model by observing where an existing mangrove forest is predicted to survive under altered local conditions. Existing forest attributes can be incorporated into LEAF (v.1.0) by updating the model input parameters and logical expressions corresponding to the user's site. Variations in forest size, density, and distribution can be used to evaluate the health of the forest and predict its long-term trajectory, where adaptation interventions may be required.

4.2. Critical modelling parameters

Sensitivity analyses using the LEAF (v.1.0) model revealed that long-term predictions of mangrove forest size and extent are most sensitive to input parameters affecting the establishment and mortality of the mangrove forest. The influence of these parameters was more

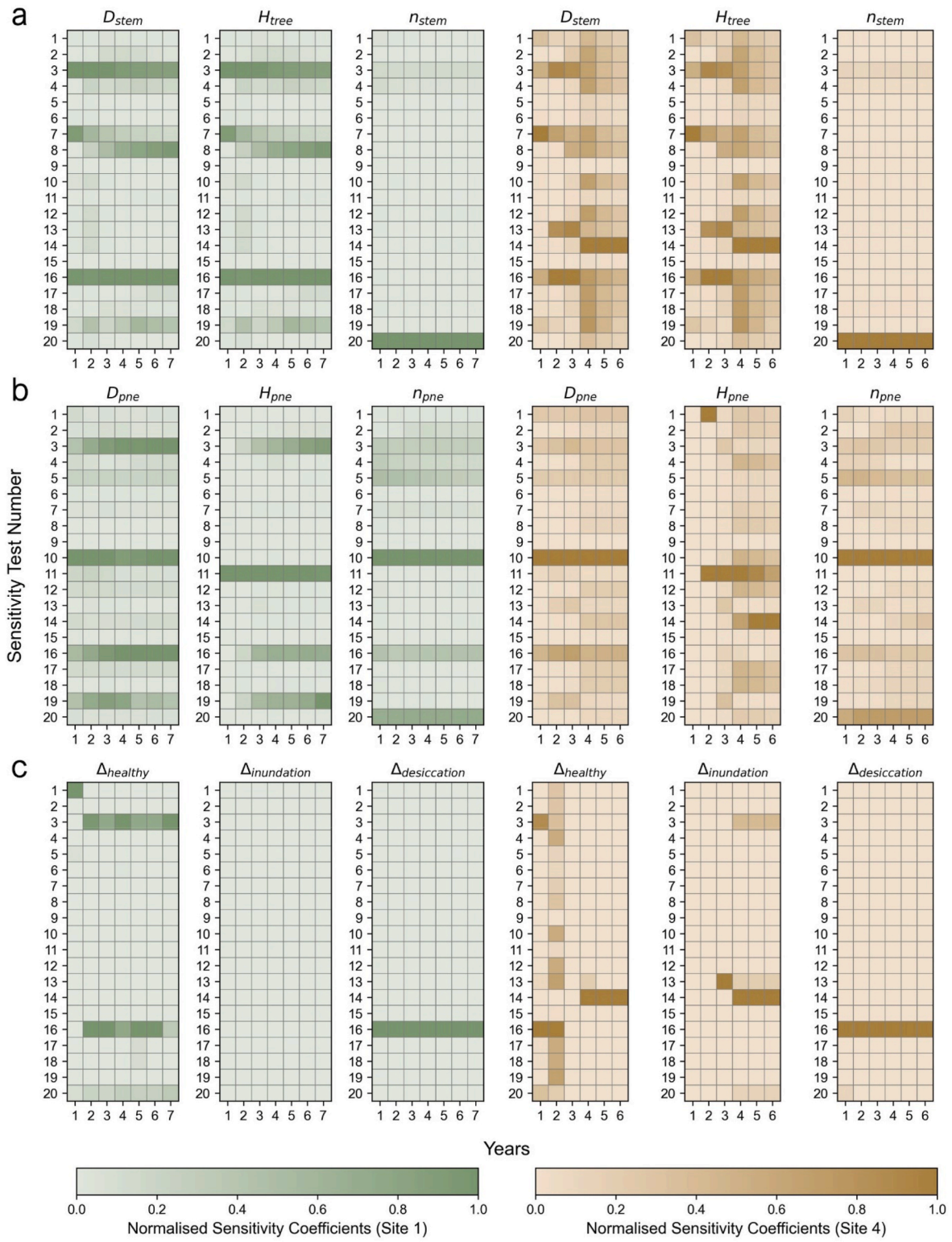

Fig. 10. Mangrove attribute sensitivity tests for every year of the model run for Site 1 (Spencer, Hawkesbury River (DRV)) (left), and Site 4 (Gerroa, Crooked River (IOCE)) (right). (a) Stem diameter, tree height, and stem density; (b) Pneumatophore diameter, height, and density; (c) Elevation difference in healthy mangrove zone, inundation zone, and desiccation zone.

pronounced at intermittently open and closed estuaries (IOCEs) versus drowned river valleys (DRVs), as mangroves in highly dynamic estuaries can experience longer periods of inundation and desiccation. The influencing establishment stage parameters, such as the fruiting window timing and inundation free period, are available in peer-reviewed literature for *Avicennia marina* and other mangrove genera. However, the magnitude and duration of inundation and desiccation causing stress and mortality of mangroves are not well understood. Long-term field and laboratory studies are recommended across the mangrove lifecycle to derive relationships that can be included in modelling tools such as the LEAF model. While the sensitivity analyses in this study were conducted by adjusting individual input parameters, compound sensitivity

testing could be conducted via Monte-Carlo simulations (Kibler et al., 2022) to understand the influence of changing multiple parameters on the model outcomes.

4.3. Advances in predictive modelling

Limited field data means that there is an inherent uncertainty in parameter values and model outputs. For this reason, the LEAF (v.1.0) model has only been validated for cross-shore extent, an attribute that has been measured extensively across different estuary typologies (Henderson and Glamore, 2024b). LEAF (v.1.0) should therefore be used as a comparison tool, rather than to provide absolute outcomes. Confidence intervals or error bars may be included for single parameter outputs, but integrating error bars for all biophysical processes will lead to complicated uncertainty propagation and may become meaningless to the user. To overcome this parameter uncertainty, probabilistic distributions of mangrove attributes and responses to hydro-morphodynamic conditions are required. These probability functions can be derived for future model revisions following the acquisition of sufficient long-term field data. With these functions, Monte Carlo simulations may be carried out to evaluate the likelihood of mangrove outputs (Kibler et al., 2022), and to help mitigate uncertainty propagation. This represents the next major step in biophysical modelling, where probabilistic estimates of mangrove predictions are used to transition the LEAF model from providing comparative results for optioneering, to predicting the likely outcomes for core mangrove attributes, such as individual stem size, density, establishment probability, and response to extreme events.

4.4. Field data acquisition

LEAF (v.1.0) has been developed for practitioners to update the model logic and input parameters with field data. Field surveys can be undertaken to derive the allometric relationships between diameter, height, and density, for both stems and pneumatophores. Like the parameters affecting mangrove mortality, these relationships have been correlated to the growth of the forest and can lead to more accurate long-term predictions. Existing growth relationships are based on limited data from the field, often for several trees at one or two sites for a single species (Mori et al., 2022; Ohira et al., 2013), or in combination with varied datasets from literature (Thampanya, 2006). Therefore, there is an opportunity for researchers to undertake detailed surveys of entire mangrove forests to expand on existing growth relationships and to fill the deficit in field data across mangrove species (Twomey and Lovelock, 2025).

Updated field data could improve the thresholds for inundation and desiccation over time in conjunction with monitored water levels and bed elevations. Mangrove failure from overturning or toppling, and breaking, could also be determined. These thresholds can be used to indicate the likelihood of mangroves dying during extreme storm events, particularly when exposed to wind and wave forces. The addition of mortality from acute climate hazards could be used to complement the long-term impacts of inundation, desiccation, and burial variables incorporated in LEAF (v.1.0). This could provide a holistic prediction of long-term mangrove development and survival in changing environmental conditions. Validation of these thresholds by investigating the forces that have caused mangrove forest failure is recommended to improve the reliability of the model outcomes.

To further strengthen the credibility of the predicted model outputs, model validation may also be carried out for metrics representative of mangrove growth, biomass accumulation, and stem density changes. This temporal validation requires periodic, long-term field measurements in the order of years to decades. Undertaking regular measurements of aboveground biomass across the mangrove lifecycle by either weighing individual mangroves (Tamai et al., 1986) or calculating biomass using a volumetric analysis (Olagoke et al., 2016), can help support predicted growth outputs. When combined with the age of the forest, the growth trajectory of individual mangroves can be determined, and used for validating mangrove growth from seedling to adult. Similarly, regular measurements of mangrove stem density can support validation of the self-thinning process in forests (Pretzsch, 2006), where competition stresses and available light sources inhibit their growth (Berger and Hildenbrandt, 2000; Beselly et al., 2023; Clarke, 1995). This self-thinning process has not been included within LEAF (v.1.0) due to current limitations with computational memory and storage associated with large matrices for an individual based model. However, with advances in computing resource efficiency and storage, and remote sensing data, future model revisions may include high densities of seedlings at the start of the model runs and the potential for the model to remove smaller trees when a threshold ratio of stem diameter to density is exceeded. To expand model validation from the nearshore environment to the estuary scale, aerial imagery of mangrove extent may be combined with on the ground measurements of bed elevation.

Improvements in technology, such as recent advances in field techniques using airborne LiDAR (Feliciano et al., 2017; Wannasiri et al., 2013) and terrestrial laser scanning (Dunlop et al., 2025; Olagoke et al., 2016), allow for the rapid acquisition of data where mangrove attributes can be processed quickly at the tree and forest scale. These field measurements can then be used to train biophysical models to understand how mangrove forests are represented in space and time, especially at a time when machine learning and artificial intelligence are being used in ecological engineering contexts to predict the capacity of vegetation to deliver ecosystem services (Cai et al., 2023; WWF, 2024). Such technological advancements can serve to better integrate the LEAF model more effectively with field data and limit the reliance on human input.

4.5. Model development

Future model revisions may expand on version 1.0 of the LEAF model to include additional functionality. Further to the inclusion of field data, the aspects of mangrove forest growth and survival can be complemented by a more detailed prediction of the establishment and growth stages. A revised establishment stage may include the probability of propagule abscission from fecund trees, as well as obligate propagule dispersal and buoyancy periods, prior to initiating root growth (Beselly et al., 2023; Gijsman et al., 2024a). A revised growth stage could also incorporate competition stresses from neighbouring trees to limit growth rates and the available space for future recruitment (Beselly et al., 2023), integrating ecological processes with the influencing hydro-morphodynamics. For each ecological process influencing these lifecycle stages, a range or distribution of values could be assigned, enabling a probabilistic rather than deterministic approach.

LEAF (v.1.0) has focused on mangrove growth in relation to hydro-morphodynamics and should only be applied in systems that have or have had mangroves previously present (e.g., where environmental conditions are favourable to mangrove growth). Future model revisions could consider ecosystem establishment and growth caused by changes to nutrient loading and salinity (Chen and Twilley, 1998), as well as other environmental variables such as pH, dissolved oxygen levels, and surface temperature (Van der Stocken et al., 2022), and biological factors such as predation (Clarke and Kerrigan, 2002), fungal pathogens, and disease (Goudarzi and Moslehi, 2020). These updates may be achieved by combining a hydro-morphodynamic model with other environmental modelling tools, such as those for water quality, catchment modelling, species competition, nutrient loading, and land-use changes.

When other modelling tools are coupled with the LEAF model, different equations may be used to represent the influence of mangroves in the model. For instance, when testing LEAF (v.1.0), the Baptist equation (Hutton et al., 2020) was utilised in the DFM model, exchanging the variables of stem diameter, height, and density, and drag coefficient (based on projected area and volume), to increase bulk roughness in grid cells with mangroves. This equation was derived based on the assumption that vegetation can be represented as vertical

cylinders. Alternative drag force formulations, including those for vegetation based on the Keulegan-Carpenter number (Cao et al., 2015; Maza et al., 2015; van Wesenbeeck et al., 2022), and those based on the flexibility of the vegetation (van Veelen et al., 2020), can be incorporated by the user. In other models, such as ROMS (Yoshikai et al., 2023) and ELCOM (van Maanen et al., 2015), the complex 3D geometry of mangroves has been further represented. The projected area of mangrove forests (Dunlop et al., 2025) and the diversity in aerial root geometry across mangrove genera, such as the stilt roots of *Rhizophora* sp., the buttress roots of *Ceriops* sp., and the knee roots of *Bruguiera* sp., may be represented in future model revisions. This would involve the inclusion of parameters to represent root growth relative to water depth, and the interactions between species when considering multi-species models. Alongside aerial root systems, branches and canopies of mangroves may be included in future LEAF model revisions, particularly in the early lifecycle stages when these elements are impacted by waves and currents with greater frequency. To this end, LEAF (v.1.0) has been developed with the aim that variables within the model code can be adjusted for alternative model coupling and mangrove representation.

4.6. Future applications

The LEAF (v.1.0) model presents a user-friendly tool to predict lifecycle changes for individual mangroves, where the outputs of mangrove size, biomass, and extent can be quantified over time. With this model functionality, users can apply LEAF (v.1.0) to the optioneering and evaluation phases of mangrove restoration and wider NbS projects (e.g., to compare different restoration strategies by monitoring the evolution of the mangrove forest post implementation). These two lifecycle phases of NbS projects have been shown to lack quantitative support for practitioners to adequately design and implement mangrove restoration works (Dunlop et al., 2023). To this aim, LEAF (v.1.0) presents an adaptable model for practitioners in any coastal environment to assess the suitability of their shoreline to mangrove growth or restoration.

Currently, LEAF (v.1.0) examines the suitability for mangrove growth on a schematised shoreline in the nearshore environment, where hydrodynamic boundary conditions have already been transformed from the offshore or upstream environment. However, to understand how the growth of a mangrove forest can impact and be impacted by the wider estuarine system, LEAF (v.1.0) would need to be applied within a large-scale estuary or coastline model, such as those achieved for saltmarsh in SCHISM (Nunez et al., 2021). In this way, the impact of anthropogenic activities such as land use changes, construction of coastal protection structures, and dredging, as well as natural processes governing offshore wave conditions, river flows, and rainfall, can be evaluated.

5. Conclusion

In this study, a mangrove Lifecycle Ecosystem Analysis and Forecasting (LEAF) model (version 1.0, dated January 31, 2025) has been developed as a user-friendly tool to predict and monitor individual mangrove and forest development over time. This model provides practitioners with the option to include relevant mangrove attributes obtained from the field or laboratory to tailor the model predictions to their site. Model outputs of LEAF (v.1.0) comprise stem and root size and density, the spatial impact of inundation, desiccation, and burial of the mangrove forest, above- and below-ground biomass calculations, and coastal protection parameters such as projected area, volume, and drag coefficient. To test the functionality of LEAF (v.1.0), the model was coupled to a hydro-morphodynamic model in Delft3D Flexible Mesh, where the response of the mangrove forest to changing water levels, bed shear stresses from waves, accretion, and erosion was observed.

The cross-shore distribution of mangrove extent was successfully predicted in four estuary typologies using long-term water level gauge data, and by modifying input parameters associated with inundation and desiccation, with high inundation thresholds aligning with the resilience of mangroves in IOCEs. A comprehensive sensitivity analysis revealed the convergence of the cross-shore distribution of mangroves under longer model runs, where the impacts of anomalous extreme events are less pronounced, and the typical extent of living mangroves can be determined. Timesteps of 12hrs or less were found to be suitable for accurately predicting mangrove establishment, in accordance with measured inundation free periods for *Avicennia marina*. The sensitivity analysis outputs identified the timing and duration of the fruiting window, the inundation free period for establishment, and the inundation depth and duration that cause mangrove stress and mortality, as critical input parameters that influence the development of the mangrove forest. These parameters were found to be more influential to mangrove forest development in constrained estuaries such as IOCEs than in DRVs, emphasising the importance of evaluating the environmental site conditions when making decisions on restoration or conservation. Results highlight the need for future research to target the magnitude and durations of critical inundation and desiccation thresholds, as well as to confirm the predicted outcomes in additional locations. The predicted outcomes of LEAF (v.1.0) should be used to inform mangrove viability and to compare restoration strategies rather than relied upon in absolute terms. Future revisions of LEAF (v.1.0) could incorporate data from field surveys to expand on available simplified allometric relationships and include failure mechanisms from storm events to cover both acute and chronic climate hazards when evaluating mangrove forest response.

CRediT authorship contribution statement

Thomas Dunlop: Conceptualization, Formal analysis, Investigation, Methodology, Software, Validation, Visualization, Writing – review & editing, Writing – original draft. **Stefan Felder:** Conceptualization, Methodology, Resources, Supervision, Writing – review & editing. **William Glamore:** Conceptualization, Methodology, Resources, Supervision, Writing – review & editing.

Software and data availability

Name of software: LEAF.
Developer: Thomas Dunlop.
Contact: t.dunlop@unsw.edu.au.
Date first available: January 31, 2025.
Software required: Delft3D Flexible Mesh.
Program language: Python, Source code at: https://github.com/DunlopT/LEAF.
Documentation: Detailed documentation for the installation, preparation, and execution of the LEAF model (including example model runs) can be found at https://github.com/DunlopT/LEAF/blob/main/README.md.
License: GPL-3.0.

Declaration of competing interest

The authors declare that they have no known competing financial interests or personal relationships that could have appeared to influence the work reported in this paper.

Acknowledgements

The first author would like to thank Bregje van Wesenbeeck (TU Delft) for the supervision and resources provided during the first author's research stay at TU Delft. The authors are grateful for the support provided by Kit Calcraft (WRL, UNSW Sydney) regarding the initial Python setup, Gijs Hendrickx (TU Delft) regarding technical Python queries and the BMI interface, Bart van Westen and Roy van Weerdenburg (both TU Delft) in the coupling of the Python model to Delft3D Flexible Mesh, and Sebrian Beselly (IHE Delft Institute for Water

Education) in the activation of the vegetation bulk roughness equation.

Supplementary Material

Supplementary data to this article can be found online at https://doi.org/10.1016/j.envsoft.2025.106619.

Appendix A. LEAF (v.1.0) model inputs

Table A.1
List of mangrove model inputs that can be updated by the user.

Model component	Input	Units/Format	Base case value	References
1. Time	1A. Timestep duration	s	43200	*Avicennia marina*; Henderson and Glamore (2024b)
	1B. Number of timesteps	–	Various	Based on continuous water level time series
	1C. Fruiting window start date	DD/MM/YYYY	Various	2-month window for *Avicennia marina* based on: Duke (1990), Jiménez (1992), Steinke (1975)
	1D. Fruiting window end date	DD/MM/YYYY	Various	2-month window for *Avicennia marina* based on: Duke (1990), Jiménez (1992), Steinke (1975)
	1E. Fruiting window annual recurrence	Y/N	Y	User defined
2. Plotting	2A. Plotting interval	No. of timesteps	120	User defined
3. Initial mangroves	3A. Initial mangrove presence	Y/N	Y	User defined
	3B. Stem density	Stems/m2	Various	User defined
	3C. Stem diameter	m	Various	User defined
	3D. Cable root length	m	Various	User defined
	3E. Cable root diameter	m	Various	User defined
	3F. Pneumatophore length	m	Various	User defined
	3G. Pneumatophore diameter	m	Various	User defined
	3H. Age	years	Various	User defined
4. Mangrove extrema	4A. Maximum stem density	Stems/m2	Various	User defined
	4B. Maximum stem height	m	Various	User defined
	4C. Maximum stem diameter	m	Various	User defined
	4D. Maximum cable root length	m	15	*Avicennia marina*; Purnobasuki et al. (2017)
	4E. Maximum cable root diameter	m	0.05	*Avicennia marina*; Based on a mean of 0.024m from Purnobasuki et al. (2017)
	4F. Maximum no. of cable roots	–	Various	User defined
	4G. Maximum pneumatophore diameter	m	0.015	*Avicennia marina* field observations and Al-Khayat and Alatalo (2021)
5. Other mangrove parameters	5A. Sapling height threshold	m	0.5	*Avicennia marina*; Clarke and Allaway (1993); Osland et al. (2015)
	5B. Fecundity age	years	1	Assumed. This is assumed to be the young adult stage as per Clarke (1995)
	5C. Cable root depth	m	0.05	User defined. Lauff (1967) found roots 0.25–0.3m below surface, and Komiyama et al. (2000) found few deeper than 0.3m
	5D. Pneumatophore spacing (based on sediment type)	m	0.04	User defined
	5E. Autochthonous accretion rate	m/year	0.004	*Avicennia marina* in NSW, Marx et al. (2020)
	5F. Starting cable/tap root length on establishment	m	0.001	User defined
	5G. Starting stem diameter on establishment	m	0.001	User defined
	5H. Starting pneumatophore diameter on growth	m	0.005	User defined
6. Establishment	6A. Establishment stage activation	Y/N	Y	User defined
	6B. Seed travel distance (neighbouring cell metric)	m	8	User defined.
	6C. Inundation free period	hrs	12	*Avicennia marina*; Henderson and Glamore (2024b)
	6D. Chance of establishment	–	0.1	Adapted from Clarke (1995)
	6E. Critical bed shear stress	N/m^2 OR formula	$\tau_{disl} = 0.4135 * RP_{max} - 0.058$ (where RP_{max} = max. root length)	*Avicennia alba* propagules in mangrove mud, Balke et al. (2015)
	6F. Cable root length requirement for stem growth	m OR formula (code adjustment required for formula)	0.005	*Avicennia marina*; Balke et al. (2015)

(*continued on next page*)

Table A.1 (*continued*)

Model component	Input	Units/Format	Base case value	References
	6G. Critical erosion limit	m OR formula (code adjustment required for formula)	$E_{crit} = 3.5058 * \ln(Sh) - 5.0584$ (where Sh is stem/shoot height)	*Avicennia marina*; Balke et al. (2015)
7. Growth	7A. Growth stage activation	Y/N	Y	User defined
	7B. Growth logic	Code adjustment required	Function that proportionally reduces growth due to stress: binary, linear, or sigmoid	van Maanen et al. (2015); van Oorschot et al. (2016); Xie et al. (2020)
	7C. Seedling stem diameter growth rate	m/day OR formula (code adjustment required for formula)	0.00004	*Avicennia marina*; Hastuti and Hastuti (2018)
	7D. Seedling stem height to diameter relationship	Number OR formula (code adjustment required for formula)	25 (i.e., stem height ~25 x stem diameter)	Based on measurements from Jacotot et al. (2019) for *Avicennia marina*
	7E. Seedling cable root growth rate	m/day OR formula (code adjustment required for formula)	0.003	*Avicennia marina*; Balke et al. (2015)
	7F. Seedling root diameter to length relationship	Number OR formula (code adjustment required for formula)	43 (i.e., root diameter ~ cable root length/43)	Based on cable root diameters of 4 species in Basyuni et al. (2018)
	7G. Sapling/adult stem diameter growth rate	m/day OR formula (code adjustment required for formula)	0.00003	Assumed based on 0.3m DBH over 30yrs for 20–25yr *Avicennia marina,* Rajkumar S. et al. (2017)
	7H. Sapling/adult stem height to diameter relationship	Number OR formula (code adjustment required for formula)	25	Value adopted to maintain transition between seedling and sapling. Alternatives for *Avicennia marina*: Thampanya (2006); Rajkumar S. et al. (2017)
	7I. Sapling/adult cable root growth rate	m/day OR formula (code adjustment required for formula)	0.001	Assumed based on 10m length in 30yrs
	7J. Sapling/adult cable root diameter to length relationship	Number OR formula (code adjustment required for formula)	Cable root diameter is 1/200 x cable root length	Assumed relationship based on 0.05m diameter in 30yrs
	7K. Pneumatophore growth condition	Proportion of pneumatophore height	1	Max. water level $\geq$ growth condition * aboveground pneumatophore height Assumed to be ≥ 1
	7L. Pneumatophore base diameter growth rate	m/day OR formula (code adjustment required for formula)	0.00001	Assumed
	7M. Ratio of pneumatophore height to base diameter	Number OR formula (code adjustment required for formula)	10.3	*Avicennia marina*; Jerez Nova (2022)
8A. Recovery and mortality - General	8A1. Recovery and mortality stage activation	Y/N	Y	User defined
8B. Recovery and mortality - Inundation	8B1. Inundation mortality activation	Y/N	Y	User defined
	8B2. Minimum depth of inundation to cause mortality	m	0.5	*Avicennia marina*; Henderson and Glamore (2024b)
	8B3. Proportion of seedling stem height inundated to initiate stress or cause mortality	–	1	Assumed
	8B4. Proportion of sapling/adult pneumatophore height inundated to initiate stress or cause mortality	–	1	Assumed
	8B5. Duration of inundation to cause stress: (i) seedlings, (ii) saplings/adults	No. of timesteps	6 (3 days)	Assumed
	8B6. Duration of inundation to cause mortality: (i) seedlings, (ii) saplings/adults	No. of timesteps	20 (10days)	Assumed
	8B7. Duration of recovery from inundation stress: (i) seedlings, (ii) saplings/adults	No. of timesteps	16 (8 days)	Assumed
	8B8. Additional recovery time (due to a second event occurring prior to full recovery): (i) seedlings, (ii) saplings/adults	No. of timesteps	10 (5 days)	Assumed
	8B9. Maximum number of inundation events limiting recovery timeframe	–	2	User defined. Limited by computational efficiency
8C. Recovery and mortality - Desiccation	8C1. Desiccation mortality activation	Y/N	Y	User defined
	8C2. Water depth threshold for desiccation	m	0.001	User defined. Dry cell threshold
	8C3. Duration of desiccation to initiate stress: (i) seedlings, (ii) saplings/adults	No. of timesteps	6 (3 days)	Assumed
	8C4. Duration of desiccation to cause mortality: (i) seedlings, (ii) saplings/adults	No. of timesteps	20 (10days)	Assumed

(*continued on next page*)

Table A.1 (*continued*)

Model component	Input	Units/Format	Base case value	References
	8C5. Duration of recovery from desiccation stress: (i) seedlings, (ii) saplings/adults	No. of timesteps	16 (8 days)	Assumed
	8C6. Additional recovery time (in the event of a second event occurring prior to full recovery): (i) seedlings, (ii) saplings/adults	No. of timesteps	10 (5 days)	Assumed
	8C7. Maximum number of desiccation events limiting recovery timeframe	–	2	User defined. Limited by computational efficiency
8D. Recovery and mortality - Burial	8D1. Burial mortality activation	Y/N	Y	User defined
	8D2. Maximum no. of timesteps over which sedimentation is assumed to be sudden (and not gradual)	No. of timesteps	14 (7 days)	Ellison (1999)
	8D3. Proportion of seedling height buried to induce stress	–	0.5	Assumed
	8D4. Proportion of seedling height buried to cause mortality	–	1	Assumed
	8D5. Proportion of pneumatophore height buried to induce stress	–	0.5	Assumed
	8D6. Proportion of pneumatophore height buried to cause mortality	–	1	Assumed
	8D7. Duration of burial required to cause mortality	No. of timesteps	60 (30 days)	Assumed
8E. Recovery and mortality - senescence	8E1. Senescence mortality activation	Y/N	Y	User defined
	8E2. Maximum age	years	100	Assumed
8F. Recovery and mortality – System removal	8F1. System removal activation	Y/N	N	User defined
	8F2. Stem height threshold for removal of dead mangroves from the system	m	0.1	User defined
9. Functionality	9A. Functionality stage activation	Y/N	Y	User defined
	9B. Projected area (stems)	m^2 OR formula (code adjustment required for formula)	Cylinder ($A = Dh$)	Assumed cylindrical front face
	9C. Projected area (pneumatophores)	m^2 OR formula (code adjustment required for formula)	Simplified: $A = Dh/2$ Detailed: $A = h/2 * [D_{90} * 0.1 + (D_{50} + D_{90}) * 0.4 + (D_0 + D_{50}) * 0.5]$ (where D_n refers to the pneumatophore diameter at n% of its height)	Simplified: front face of a cone as adopted for *Avicennia marina* pneumatophores, Du et al. (2021) Detailed: Pneumatophore model for *Avicennia marina* from Jerez Nova (2022) with 2 frustums and one cone
	9D. Projected volume (stems)	m^3 OR formula (code adjustment required for formula)	Cylinder ($V = \pi D^2 h/4$)	Assumed cylindrical stem beneath water level
	9E. Projected volume (pneumatophores)	m^3 OR formula (code adjustment required for formula)	Simplified: $V = \pi D^2 h/12$ Detailed: $V = \pi h/12 * [D_{50}^2 * (0.1) + (D_{50}^2 - D_{50}^2) * (0.4) + (D_0^2 - D_{50}^2) * (0.5)]$ (where D_n refers to the pneumatophore diameter at n% of its height)	Simplified: Volume of a cone as adopted for *Avicennia marina* pneumatophores, Du et al. (2021) Detailed: Pneumatophore model for *Avicennia marina* from Jerez Nova (2022) with 2 frustums and one cone.
	9F. Drag coefficient	Number OR formula (code adjustment required for formula)	$C_d = 0.005 + 5/L$ (where $L = (V - V_m)/A$, and V_m is the control volume)	van Maanen et al. (2015), Mazda et al. (1997), and Mazda et al. (2005). Alternative equation provided by van Hespen et al. (2021)
	9G. Percentile of stem heights and diameters in each grid cell that are returned to DFM	–	85	User defined
	9H. Biomass activation	Y/N	Y	User defined
	9I. Above-ground biomass	kg OR formula (code adjustment required for formula)	$AGB = 0.308 * DBH^{2.11}$	*Avicennia marina;* Comley and McGuinness (2005); Komiyama et al. (2005); Fu and Wu (2011)
	9J. Below-ground biomass	kg OR formula (code adjustment required for formula)	$BGB = 1.28 * DBH^{1.17}$	*Avicennia marina;* Comley and McGuinness (2005); Komiyama et al. (2005)
	9K. Autochthonous accretion activation	Y/N	Y	User defined

Appendix B. LEAF (v.1.0) logic diagrams

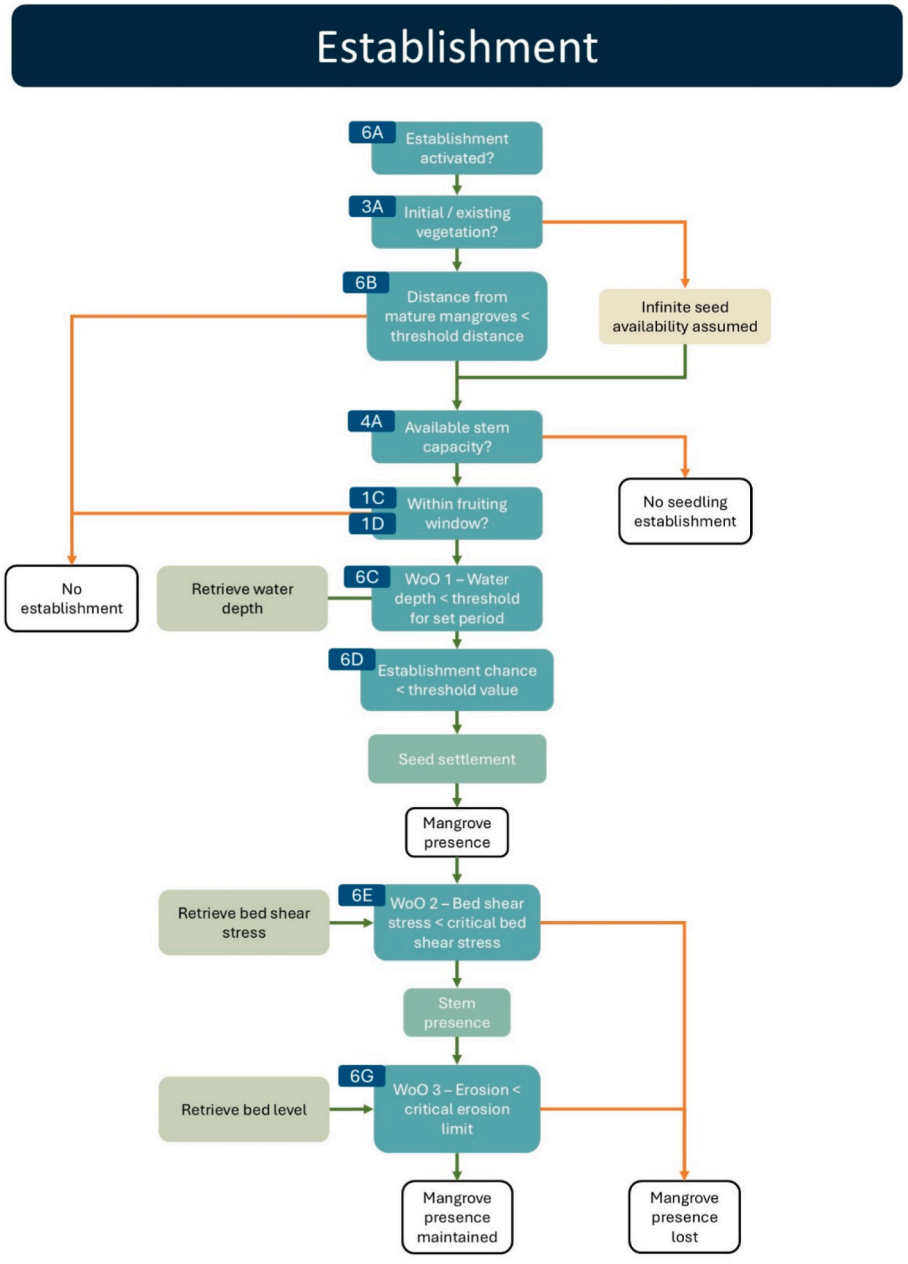

ID	Input parameter
1C	Fruiting window start date
1D	Fruiting window end date
3A	Initial mangrove presence
4A	Maximum stem density
6A	Establishment stage activation
6B	Seed travel distance
6C	Inundation free period
6D	Chance of establishment
6E	Critical bed shear stress
6G	Critical erosion limit

Fig. B.1. LEAF (v.1.0) logic flow diagram for the establishment stage.

ID	Input parameter	ID	Input parameter
4B	Maximum stem height	7B	Growth logic
4C	Maximum stem diameter	7C	Seedling stem diameter growth rate
4D	Maximum cable root length	7D	Seedling stem height to diameter relationship
4E	Maximum cable root diameter	7E	Seedling cable root growth rate
4G	Maximum pneumatophore diameter	7F	Seedling root diameter to length relationship
5A	Sapling height threshold	7G	Sapling/adult stem diameter growth rate
5D	Pneumatophore spacing	7H	Sapling/adult stem height to diameter relationship
5F	Starting cable/tap root length	7I	Sapling/adult cable root growth rate
5G	Starting stem diameter	7J	Sapling/adult cable root diameter to length relationship
5H	Starting pneumatophore diameter	7K	Pneumatophore growth condition
6F	Cable root length requirement	7L	Pneumatophore base diameter growth rate
7A	Growth stage activation	7M	Ratio of pneumatophore height to base diameter

Fig. B.2. LEAF (v.1.0) logic flow diagram for the growth stage.

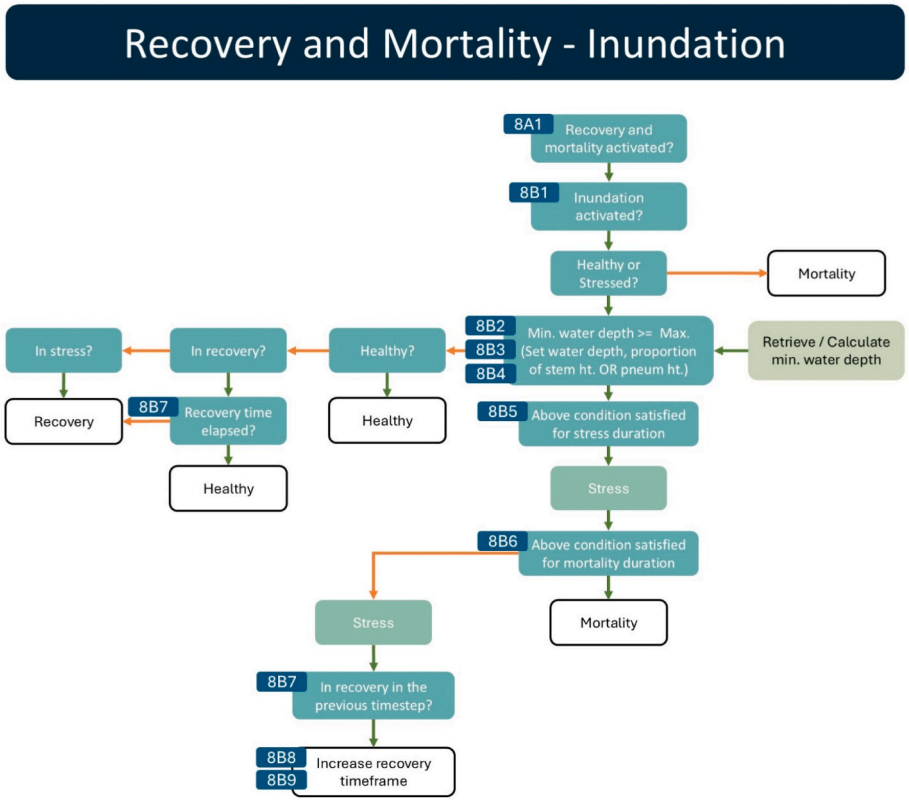

ID	Input parameter
8A1	Recovery and mortality stage activation
8B1	Inundation mortality activation
8B2	Min. inundation depth to cause mortality
8B3	Proportion of stem height inundated
8B4	Proportion of pneum. height inundated
8B5	Duration of inundation to cause stress
8B6	Duration of inundation to cause mortality
8B7	Duration of recovery from inundation stress
8B8	Additional recovery time for repeated events
8B9	Max. number of inundation events

Fig. B.3. LEAF (v.1.0) logic flow diagram for inundation in the recovery and mortality stage.

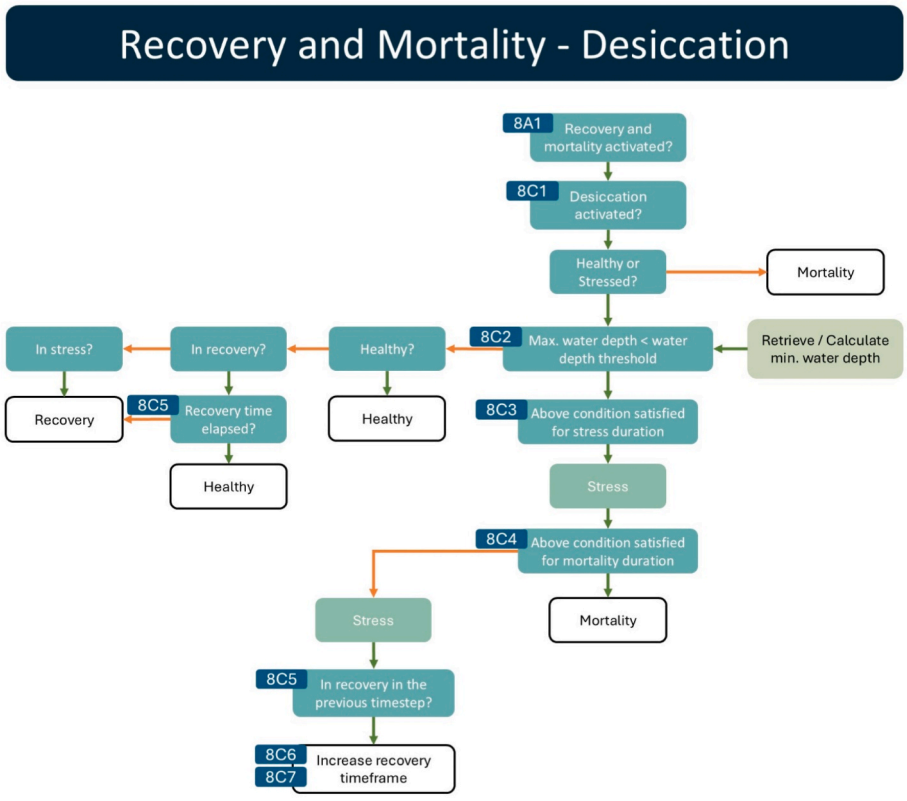

ID	Input parameter
8A1	Recovery and mortality stage activation
8C1	Desiccation mortality activation
8C2	Water depth threshold for desiccation
8C3	Duration of desiccation to cause stress
8C4	Duration of desiccation to cause mortality
8C5	Duration of recovery from desiccation stress
8C6	Additional recovery time for repeated events
8C7	Max. number of desiccation events

Fig. B.4. LEAF (v.1.0) logic flow diagram for desiccation in the recovery and mortality stage.

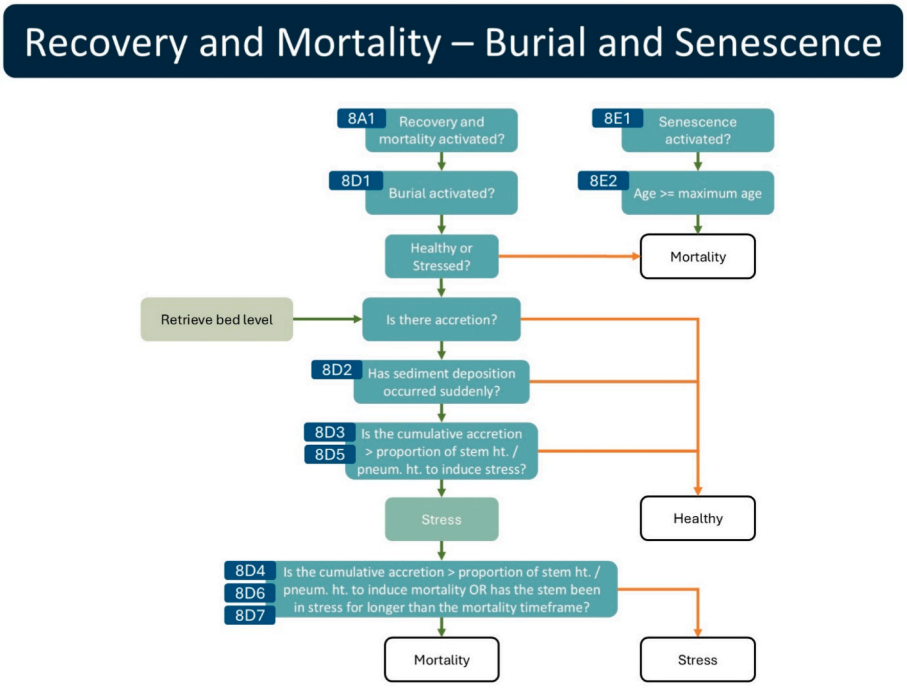

ID	Input parameter
8A1	Recovery and mortality stage activation
8D1	Burial mortality activation
8D2	Max. number of timesteps for burial event timeframe
8D3	Proportion of stem height buried to induce stress
8D4	Proportion of stem height buried to cause mortality
8D5	Proportion of pneum. height buried to induce stress
8D6	Proportion of pneum. height buried to cause mortality
8D7	Duration of burial to cause mortality
8E1	Senescence mortality activation
8E2	Maximum mangrove age

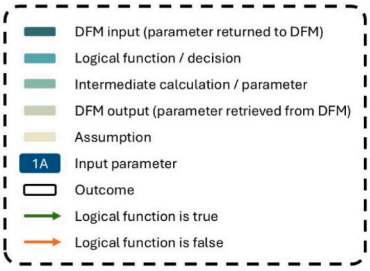

Fig. B.5. LEAF (v.1.0) logic flow diagram for burial and senescence in the recovery and mortality stage.

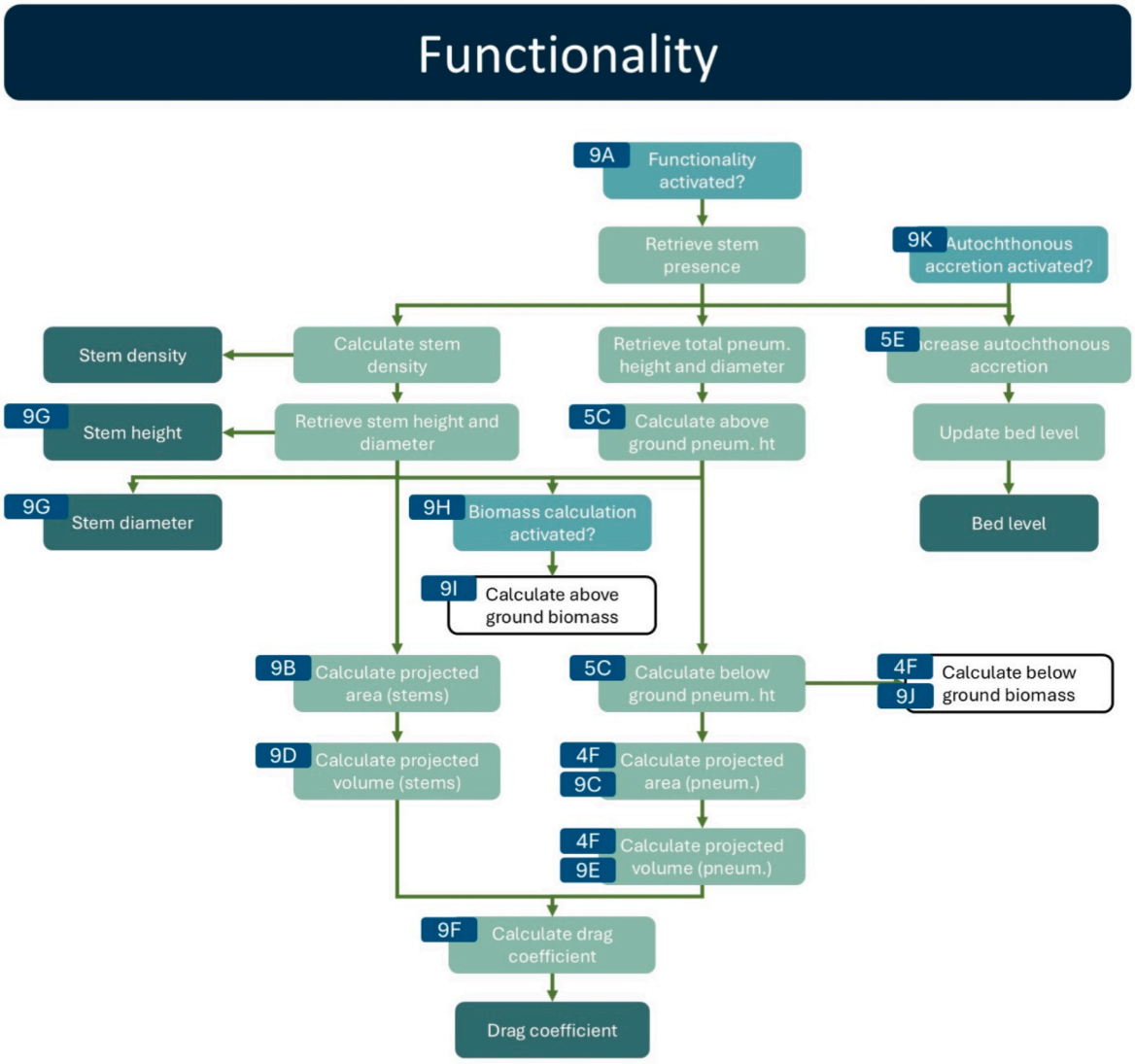

ID	Input parameter
4F	Maximum number of cable roots
5C	Cable root depth
9A	Functionality stage activation
9B	Projected area (stems)
9C	Projected area (pneumatophores)
9D	Projected volume (stems)
9E	Projected volume (pneumatophores)
9F	Drag coefficient
9G	Percentile of stem attributes returned to DFM
9H	Biomass activation
9I	Above-ground biomass
9J	Below-ground biomass
9K	Autochthonous accretion activation

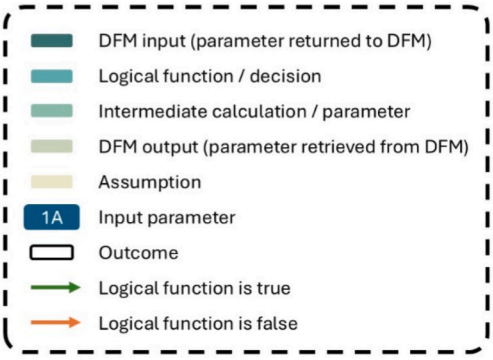

Fig. B.6. LEAF (v.1.0) logic flow diagram for the functionality stage.

Appendix C. Sensitivity tests

Table C.1
List of sensitivity tests.

Sensitivity Test	Parameter	Base case value	Sensitivity value	References	Sensitivity observed in past vegetation modelling studies
ST1	Fruiting window duration	2months	4months	Duke (1990); Jiménez (1992); Gladstone-Gallagher et al. (2014); Steinke (1975)	Increased vegetation cover for longer window for willow trees (van Oorschot et al., 2017)
ST2	Sapling height	0.5m	1m	Clarke and Allaway (1993)	N/A
ST3	Inundation free period	12hrs	24hrs	Henderson and Glamore (2024b); Balke et al. (2015)	Hydroperiod tested instead, yielding higher bed level increase for a wider period (Xie et al., 2020)
ST4	Establishment chance	0.10	0.05	Adapted from Clarke (1995)	Not tested, but adopted for saltmarsh (Willemsen et al., 2022)
ST5	Seedling root growth rate	0.03 m/d	0.01 m/d	Balke et al. (2015)	N/A
ST6	Tap root threshold for stem growth	0.005m	0.02m	Balke et al. (2015)	N/A
ST7	Seedling diameter growth rate	0.00004 m/d	0.0001 m/d	Hastuti and Hastuti (2018)	N/A
ST8	Sapling/young adult diameter growth rate	0.00003 m/d	0.000002 m/d	Rajkumar S. et al. (2017); Nazim et al. (2013)	N/A
ST9	Sapling/young adult cable root growth rate	0.001 m/d	0.003 m/d	Assumed, based on 10m length in 30yrs	N/A
ST10	Pneumatophore spacing	0.04m	0.02m	Dunlop et al. (2025)	Maximum number of root elements modified, with higher numbers yielding profile progradation at seaward edge (Xie et al., 2020)
ST11	Pneumatophore diameter growth rate	0.00001 m/d	0.00005 m/d	Assumed	N/A
ST12	Proportion of seedling stem height and pneumatophore length for inundation mortality	1	0.5	Henderson and Glamore (2024b)	Higher thresholds lead to increased stem density and reduced erosion for saltmarsh (Best et al., 2018)
ST13	Inundation timing for mortality	10days	5days	Henderson and Glamore (2024b)	Higher areal cover for knotweed (van Oorschot et al., 2016)
ST14	Inundation depth	0.5m	0.75m	Henderson and Glamore (2024b)	Included but without sensitivity (Xie et al., 2022)
ST15	Desiccation water depth threshold	0.0001m	0.001m	Assumed	N/A
ST16	Desiccation timing for mortality	10days	5days	Assumed	Higher areal cover for knotweed (van Oorschot et al., 2016)
ST17	Desiccation timing for recovery	8days	4days	Assumed	N/A
ST18	Additional desiccation timing for recovery from repeated events	5days	2.5days	Assumed	N/A
ST19	Percentile of parameter values represented in each grid cell	85th	50th	Assumed	N/A
ST20	Stem density	2stems/m^2	5stems/m^2	Assumed	Increased stem density leads to gradual propagation of shoreline edge for saltmarsh (Best et al., 2018)
ST21	Fruiting window timing	15-01 to 15-03	15-03 to 15-05	Duke (1990)	N/A
ST22	Fruiting window timing	15-01 to 15-03	15-05 to 15-07	Duke (1990)	N/A
ST23	Fruiting window timing	15-01 to 15-03	15-07 to 15-09	Duke (1990)	N/A
ST24	Fruiting window timing	15-01 to 15-03	15-09 to 15-11	Duke (1990)	N/A
ST25	Fruiting window timing	15-01 to 15-03	15-11 to 15-01	Duke (1990)	N/A

Data availability

The continuous water level time series data used in this study are available at https://zenodo.org/records/14870553.

References

Al-Khayat, J.A., Alatalo, J.M., 2021. Relationship between tree size, sediment mud content, oxygen levels, and pneumatophore abundance in the mangrove tree species Avicennia marina (forssk.) vierh. J. Mar. Sci. Eng. 9 (1).

Alongi, D.M., 2014. Carbon cycling and storage in mangrove forests. Ann. Rev. Mar. Sci 6, 195–219. https://doi.org/10.1146/annurev-marine-010213-135020.

Balke, T., Bouma, T.J., Horstman, E.M., Webb, E.L., Erftemeijer, P.L.A., Herman, P.M.J., 2011. Windows of opportunity: thresholds to mangrove seedling establishment on tidal flats. Mar. Ecol. Prog. Ser. 440, 1–9. https://www.int-res.com/abstracts/meps/v440/p1-9/.

Balke, T., Swales, A., Lovelock, C.E., Herman, P.M.J., Bouma, T.J., 2015. Limits to seaward expansion of mangroves: translating physical disturbance mechanisms into seedling survival gradients. J. Exp. Mar. Biol. Ecol. 467, 16–25. https://doi.org/10.1016/j.jembe.2015.02.015.

Baptist, M.J., Babovic, V., Rodríguez Uthurburu, J., Keijzer, M., Uittenbogaard, R.E., Mynett, A., Verwey, A., 2007. On inducing equations for vegetation resistance. J. Hydraul. Res. 45 (4), 435–450. https://doi.org/10.1080/00221686.2007.9521778.

Basyuni, M., Keliat, D.A., Lubis, M.U., Manalu, N.B., Syuhada, A., Wati, R., Yunasfi, 2018. Growth and root development of four mangrove seedlings under varying salinity. IOP Conf. Ser. Earth Environ. Sci. 130 (1), 012027. https://doi.org/10.1088/1755-1315/130/1/012027.

Berger, U., Hildenbrandt, H., 2000. A new approach to spatially explicit modelling of forest dynamics: spacing, ageing and neighbourhood competition of mangrove trees. Ecol. Model. 132 (3), 287–302. https://doi.org/10.1016/S0304-3800(00)00298-2.

Beselly, S.M., Grueters, U., van Der Wegen, M., Reyns, J., Dijkstra, J., Roelvink, D., 2023. Modelling mangrove-mudflat dynamics with a coupled individual-based-hydro-morphodynamic model. Environ. Model. Software 169, 105814. https://doi.org/10.1016/j.envsoft.2023.105814.

Best, U., van der Wegen, M., Reyns, J., Dijkstra, J., Roelvink, D., 2021. *Multi-Time Scale Mangrove-Mudflat Modelling: Exploring Guyana's Unique Dataset & Numerical Modelling* Coastal Dynamics 2021.

Best, Ü.S.N., Van der Wegen, M., Dijkstra, J., Willemsen, P.W.J.M., Borsje, B.W., Roelvink, D.J.A., 2018. Do salt marshes survive sea level rise? Modelling wave action, morphodynamics and vegetation dynamics. Environ. Model. Software 109, 152–166. https://doi.org/10.1016/j.envsoft.2018.08.004.

Brückner, M.Z.M., Schwarz, C., van Dijk, W.M., van Oorschot, M., Douma, H., Kleinhans, M.G., 2019. Salt marsh establishment and eco-engineering effects in dynamic estuaries determined by species growth and mortality. J. Geophys. Res.: Earth Surf. 124 (12), 2962–2986. https://doi.org/10.1029/2019JF005092.

Cai, L., Kreft, H., Taylor, A., Denelle, P., Schrader, J., Essl, F., van Kleunen, M., Pergl, J., Pyšek, P., Stein, A., Winter, M., Barcelona, J.F., Fuentes, N., Inderjit, Karger, D.N., Kartesz, J., Kuprijanov, A., Nishino, M., Nickrent, D., Weigelt, P., 2023. Global models and predictions of plant diversity based on advanced machine learning techniques. New Phytol. 237 (4), 1432–1445. https://doi.org/10.1111/nph.18533.

Cao, H., Chen, Y., Tian, Y., Feng, W., 2015. Field investigation into wave attenuation in the mangrove environment of the South China Sea Coast. J. Coast Res. 32 (6), 1417–1427. https://doi.org/10.2112/JCOASTRES-D-15-00124.1.

Caponi, F., Vetsch, D.F., Vanzo, D., 2023. BASEveg: a python package to model riparian vegetation dynamics coupled with river morphodynamics. SoftwareX 22, 101361. https://doi.org/10.1016/j.softx.2023.101361.

Chen, R., Twilley, R.R., 1998. A gap dynamic model of mangrove forest development along gradients of soil salinity and nutrient resources. J. Ecol. 86 (1), 37–51. https://doi.org/10.1046/j.1365-2745.1998.00233.x.

Choy, S.C., Booth, W.E., 1994. Prolonged inundation and ecological changes in an avicennia mangrove: implications for conservation and management. Hydrobiologia 285 (1), 237–247. https://doi.org/10.1007/BF00005670.

Clarke, P.J., 1995. The population dynamics of the mangrove avicennia marina; demographic synthesis and predictive modelling. Hydrobiologia 295 (1), 83–88. https://doi.org/10.1007/BF00029114.

Clarke, P.J., Allaway, W.G., 1993. The regeneration niche of the grey mangrove (avicennia marina): effects of salinity, light and sediment factors on establishment, growth and survival in the field. Oecologia 93 (4), 548–556. https://doi.org/10.1007/BF00328964.

Clarke, P.J., Kerrigan, R.A., 2002. The effects of seed predators on the recruitment of mangroves. J. Ecol. 90 (4), 728–736. https://doi.org/10.1046/j.1365-2745.2002.00705.x.

Comley, B.W.T., McGuinness, K.A., 2005. Above- and below-ground biomass, and allometry, of four common northern Australian mangroves. Aust. J. Bot. 53 (5), 431–436. https://doi.org/10.1071/BT04162.

Deitrick, A.R., Hovendon, E.H., Ralston, D.K., Nepf, H., 2023. The influence of vegetation-generated turbulence on deposition in emergent canopies [Original Research]. Front. Mar. Sci. 10. https://www.frontiersin.org/journals/marine-science/articles/10.3389/fmars.2023.1266241.

Deltares, 2020a. D-Morphology, 1D/2D/3D, User Manual (Delft3D FM Suite 2020, Issue.

Deltares, 2020b. D-Waves, User Manual (Delft3D FM Suite 2020, Issue 1.2).

Deltares, 2021. Delft3D flexible mesh suite (Delft3D FM). In: Version 2021.03) Deltares. https://www.deltares.nl/en/software-and-data/products/delft3d-flexible-mesh-suite.

Du, Q., Qin, Z., Ming, S., Zhang, C., 2021. Differences in the vertical accretion of sediment among mangrove species with different aerial root types. Estuar. Coast Shelf Sci. 256, 107375. https://doi.org/10.1016/j.ecss.2021.107375.

Duke, N.C., 1990. Phenological trends with latitude in the mangrove tree Avicennia marina. J. Ecol. 78 (1), 113–133. https://doi.org/10.2307/2261040.

Duke, N.C., 1991. A systematic revision of the mangrove genus avicennia (avicenniaceae) in australasia. Aust. Syst. Bot. 4 (2), 299–324. https://doi.org/10.1071/SB9910299.

Dunlop, T., Mancheño, A.G., Glamore, W., Felder, S., van Wesenbeeck, B.K., 2025. Quantifying mangrove forest attributes using terrestrial laser scanning. Estuaries Coasts 48 (4), 108. https://doi.org/10.1007/s12237-025-01533-0.

Dunlop, T., Glamore, W., Felder, S., 2023. Restoring estuarine ecosystems using nature-based solutions: towards an integrated eco-engineering design guideline. Sci. Total Environ. 873, 162362. https://doi.org/10.1016/j.scitotenv.2023.162362.

Dzimballa, S., Willemsen, P.W.J.M., Kitsikoudis, V., Borsje, B.W., Augustijn, D.C.M., 2025. Numerical modelling of biogeomorphological processes in salt marsh development: do short-term vegetation dynamics influence long-term development? Geomorphology 471, 109534. https://doi.org/10.1016/j.geomorph.2024.109534.

Ellison, J.C., 1999. Impacts of sediment burial on mangroves. Mar. Pollut. Bull. 37 (8), 420–426. https://doi.org/10.1016/S0025-326X(98)00122-2.

Faunce, C.H., Serafy, J.E., 2006. Mangroves as fish habitat: 50 years of field studies. Mar. Ecol. Prog. Ser. 318, 1–18. https://www.int-res.com/abstracts/meps/v318/p1-18/.

Feliciano, E.A., Wdowinski, S., Potts, M.D., Lee, S.-K., Fatoyinbo, T.E., 2017. Estimating mangrove canopy height and above-ground biomass in the everglades national park with airborne LiDAR and TanDEM-X data. Remote Sens. 9 (7).

Fu, W., Wu, Y., 2011. Estimation of aboveground biomass of different mangrove trees based on canopy diameter and tree height. Procedia Environ. Sci. 10, 2189–2194. https://doi.org/10.1016/j.proenv.2011.09.343.

Gijsman, R., Horstman, E.M., Swales, A., Balke, T., Willemsen, P.W.J.M., van der Wal, D., Wijnberg, K.M., 2024a. Biophysical modeling of mangrove seedling establishment and survival across an elevation gradient with forest zones. J. Geophys. Res.: Earth Surf. 129 (5), e2024JF007664. https://doi.org/10.1029/2024JF007664.

Gijsman, R.H.E.M., Swales, A., MacDonald, I.T., Bouma, T.J., van der Wal, D., Wijnberg, K.M., 2024b. Mangrove forest drag and bed stabilisation effects on intertidal flat morphology. Earth Surf. Process. Landf. 49 (3), 1117–1134. https://doi.org/10.1002/esp.5758.

Gladstone-Gallagher, R.V., Lundquist, C.J., Pilditch, C.A., 2014. Mangrove (Avicennia marina subsp. australasica) litter production and decomposition in a temperate Estuary. N. Z. J. Mar. Freshw. Res. 48 (1), 24–37. https://doi.org/10.1080/00288330.2013.827124.

Goudarzi, A., Moslehi, M., 2020. Distribution of a devastating fungal pathogen in mangrove forests of southern Iran. Crop Prot. 128, 104987. https://doi.org/10.1016/j.cropro.2019.104987.

Hanslow, D.J., Morris, B.D., Foulsham, E., Kinsela, M.A., 2018. A regional scale approach to assessing current and potential future exposure to tidal inundation in different types of estuaries. Sci. Rep. 8 (1), 7065. https://doi.org/10.1038/s41598-018-25410-y.

Hastuti, E.D., Hastuti, R.B., 2018. Growth characteristics of mangrove seedling in silvofishery pond – the allometric relationship of height, diameter and leaf abundance. IOP Conf. Ser. Earth Environ. Sci. 130 (1), 012015. https://doi.org/10.1088/1755-1315/130/1/012015.

Henderson, B., Glamore, W., 2024a. A lifecycle model approach for predicting mangrove extent. Sci. Total Environ. 952, 175962. https://doi.org/10.1016/j.scitotenv.2024.175962.

Henderson, B., Glamore, W., 2024b. Mangrove extent reflects estuarine typology and lifecycle events. Estuar. Coast Shelf Sci. 304, 108813. https://doi.org/10.1016/j.ecss.2024.108813.

Hendrickx, G.G., Herman, P.M.J., Dijkstra, J.T., Storlazzi, C.D., Toth, L.T., 2021. Online-coupling of widely-ranged timescales to model coral reef development. Environ. Model. Software 143, 105103. https://doi.org/10.1016/j.envsoft.2021.105103.

Hutton, E.W.H., Piper, Mark D., Tucker, Gregory E., 2020. The basic model interface 2.0: a standard interface for coupling numerical models in the geosciences. J. Open Source Softw. https://doi.org/10.21105/joss.02317.

Jacotot, A., Marchand, C., Allenbach, M., 2019. Increase in Growth and Alteration of C:N Ratios of Avicennia marina and Rhizophora stylosa Subject to Elevated CO2 Concentrations and Longer Tidal Flooding Duration [Original Research]. Frontiers in Ecology and Evolution 7. https://www.frontiersin.org/articles/10.3389/fevo.2019.00098.

Jerez Nova, K., 2022. Geometrical Mangrove Models TU Delft]. Delft, the Netherlands. https://repository.tudelft.nl/islandora/object/uuid:7b6cb673-88e2-45b2-9a30-488575b2e6cd.

Jiménez, J.A., 1992. 16 - mangrove forests of the Pacific Coast of central America. In: Seeliger, U. (Ed.), Coastal Plant Communities of Latin America. Academic Press, pp. 259–267. https://doi.org/10.1016/B978-0-08-092567-7.50022-2.

Kennedy, D.M., McSweeney, S.L., Mariani, M., Zavadil, E., 2020. The geomorphology and evolution of intermittently open and closed estuaries in large embayments in Victoria, Australia. Geomorphology 350, 106892. https://doi.org/10.1016/j.geomorph.2019.106892.

Kernkamp, H.W.J., Van Dam, A., Stelling, G.S., de Goede, E.D., 2011. Efficient scheme for the shallow water equations on unstructured grids with application to the Continental shelf. Ocean Dyn. 61 (8), 1175–1188. https://doi.org/10.1007/s10236-011-0423-6.

Kibler, K.M., 2022. Hydrodynamic limitations to mangrove seedling retention in subtropical estuaries. Flow-Biota Interaction and Natural Infrastructure Design.

Komiyama, A., Havanond, S., Srisawatt, W., Mochida, Y., Fujimoto, K., Ohnishi, T., Ishihara, S., Miyagi, T., 2000. Top/Root biomass ratio of a secondary mangrove (Ceriops tagal (perr.) C.B. rob.) forest. For. Ecol. Manag. 139 (1), 127–134. https://doi.org/10.1016/S0378-1127(99)00339-4.

Komiyama, A., Poungparn, S., Kato, S., 2005. Common allometric equations for estimating the tree weight of mangroves. J. Trop. Ecol. 21 (4), 471–477. https://doi.org/10.1017/S0266467405002476.

Lauff, G.H., 1967. Estuaries. American Association for the Advancement of Science, University of Georgia. Marine Institute. https://books.google.com.au/books?id=p5jSAAAAMAAJ.

Lovelock, C.E., Bennion, V., Grinham, A., Cahoon, D.R., 2011. The role of surface and subsurface processes in keeping pace with sea level rise in intertidal wetlands of moreton Bay, Queensland, Australia. Ecosystems 14 (5), 745–757. https://doi.org/10.1007/s10021-011-9443-9.

Manly Hydraulics Laboratory, 2024. NSW water level data collection program. Retrieved 16/01/2024 from. https://mhl.nsw.gov.au/Data-Level.

Marx, S.K., Knight, J.M., Dwyer, P.G., Child, D.P., Hotchkis, M.A.C., Zawadzki, A., 2020. Examining the response of an eastern Australian mangrove forest to changes in hydro-period over the last century. Estuar. Coast Shelf Sci. 241, 106813. https://doi.org/10.1016/j.ecss.2020.106813.

Maza, M., Lara, J.L., Losada, I.J., Ondiviela, B., Trinogga, J., Bouma, T.J., 2015. Large-scale 3-D experiments of wave and current interaction with real vegetation. Part 2: experimental analysis. Coast. Eng. 106, 73–86. https://doi.org/10.1016/j.coastaleng.2015.09.010.

Mazda, Y., Kobashi, D., Okada, S., 2005. Tidal-scale hydrodynamics within mangrove swamps. Wetl. Ecol. Manag. 13 (6), 647–655. https://doi.org/10.1007/s11273-005-0613-4.

Mazda, Y., Wolanski, E., King, B., Sase, A., Ohtsuka, D., Magi, M., 1997. Drag force due to vegetation in mangrove swamps. Mangroves Salt Marshes 1 (3), 193–199. https://doi.org/10.1023/A:1009949411068.

Menéndez, P., Losada, I.J., Torres-Ortega, S., Narayan, S., Beck, M.W., 2020. The global flood protection benefits of mangroves. Sci. Rep. 10 (1), 4404. https://doi.org/10.1038/s41598-020-61136-6.

Miedema Brown, L., Anand, M., 2022. Plant functional traits as measures of ecosystem service provision. Ecosphere 13 (2), e3930. https://doi.org/10.1002/ecs2.3930.

Mori, N., Chang, C.-W., Inoue, T., Akaji, Y., Hinokidani, K., Baba, S., Takagi, M., Mori, S., Koike, H., Miyauchi, M., Suganuma, R., Sabunas, A., Miyashita, T., Shimura, T., 2022. Parameterization of Mangrove Root Structure of Rhizophora stylosa in Coastal Hydrodynamic Model [Original Research]. Frontiers in Built Environment 7. https://www.frontiersin.org/article/10.3389/fbuil.2021.782219.

Morris, B., Foulsham, E., Hanslow, D., 2013. *Quantifying Tidal Inundation Variations in NSW Estuaries* NSW Coastal Conference 2013, Port Macquarie. NSW, Australia. https://www.coastalconference.com/2013/papers2013/Brad%20Morris%20Full%20Paper.pdf.

Mumby, P.J., Edwards, A.J., Ernesto Arias-González, J., Lindeman, K.C., Blackwell, P.G., Gall, A., Gorczynska, M.I., Harborne, A.R., Pescod, C.L., Renken, H., C, C., Wabnitz, C., Llewellyn, G., 2004. Mangroves enhance the biomass of coral reef fish communities in the Caribbean. Nature 427 (6974), 533–536. https://doi.org/10.1038/nature02286.

Nazim, K., Ahmed, M., Shaukat, S.S., Khan, M.U., Ali, Q.M., 2013. Age and growth rate estimation of grey mangrove Avicennia marina (forsk.) vierh from Pakistan. Pakistan J. Bot. 45 (2), 535–542.

Nunez, K., Zhang, Y.J., Bilkovic, D.M., Hershner, C., 2021. Coastal setting determines tidal marsh sustainability with accelerating sea-level rise. Ocean Coast Manag. 214, 105898. https://doi.org/10.1016/j.ocecoaman.2021.105898.

Ohira, W., Honda, K., Nagai, M., Ratanasuwan, A., 2013. Mangrove stilt root morphology modeling for estimating hydraulic drag in tsunami inundation simulation. Trees (Berl.) 27 (1), 141–148. https://doi.org/10.1007/s00468-012-0782-8.

Okello, J.A., Kairo, J.G., Dahdouh-Guebas, F., Beeckman, H., Koedam, N., 2020. Mangrove trees survive partial sediment burial by developing new roots and adapting their root, branch and stem anatomy. Trees (Berl.) 34 (1), 37–49. https://doi.org/10.1007/s00468-019-01895-6.

Olagoke, A., Proisy, C., Féret, J.-B., Blanchard, E., Fromard, F., Mehlig, U., de Menezes, M.M., dos Santos, V.F., Berger, U., 2016. Extended biomass allometric equations for large mangrove trees from terrestrial LiDAR data. Trees (Berl.) 30 (3), 935–947. https://doi.org/10.1007/s00468-015-1334-9.

Osland, M.J., Day, R.H., From, A.S., McCoy, M.L., McLeod, J.L., Kelleway, J.J., 2015. Life stage influences the resistance and resilience of Black mangrove forests to winter climate extremes. Ecosphere 6 (9), art160. https://doi.org/10.1890/ES15-00042.1.

Paling, E.I., Kobryn, H.T., Humphreys, G., 2008. Assessing the extent of mangrove change caused by cyclone vance in the eastern exmouth gulf, northwestern Australia. Estuar. Coast Shelf Sci. 77 (4), 603–613. https://doi.org/10.1016/j.ecss.2007.10.019.

Pretzsch, H., 2006. Species-specific allometric scaling under self-thinning: evidence from long-term plots in forest stands. Oecologia 146 (4), 572–583. https://doi.org/10.1007/s00442-005-0126-0.

Purnobasuki, H., Purnama, P., Kobayashi, K., 2017. Morphology of four root types and anatomy of root-root junction in relation gas pathway of Avicennia marina (forsk) vierh roots. Vegetos- An International Journal of Plant Research 30, 100. https://doi.org/10.5958/2229-4473.2017.00143.4.

Quartel, S., Kroon, A., Augustinus, P.G.E.F., Van Santen, P., Tri, N.H., 2007. Wave attenuation in coastal mangroves in the red river Delta, Vietnam. J. Asian Earth Sci. 29 (4), 576–584. https://doi.org/10.1016/j.jseaes.2006.05.008.

Rajkumar, S.Y., Ketan, Mewada, Salvi, Harshad, R.D., Kamboj, 2017. Age and growth relation of mangrove Avicennia marina (forssk.) vierh. In gulf of kachchh (gok), India. Appl. Sci. Rep 17 (1).

Steinke, T., 1975. Some factors affecting dispersal and establishment of propagules of Avicennia marina (forsk.) vierh. In: Proceedings of the International Symposium in Biology and Management of Mangroves.

Suzuki, T., Zijlema, M., Burger, B., Meijer, M.C., Narayan, S., 2012. Wave dissipation by vegetation with layer schematization in SWAN. Coast. Eng. 59 (1), 64–71. https://doi.org/10.1016/j.coastaleng.2011.07.006.

Tamai, S., Nakasuga, T., Tabuchi, R., Ogino, K., 1986. Standing biomass of mangrove forests in southern Thailand. J. Jpn. For. Soc. 68 (9), 384–388. https://doi.org/10.11519/jjfs1953.68.9_384.

Thampanya, U., 2006. *Mangroves and Sediment Dynamics Along the Coasts of Southern Thailand* [Doctoral Thesis, Wageningen University]. https://edepot.wur.nl/39452.

Toma, T., Nakamura, K., Patanaponpaiboon, P., Ogino, K., 1991. Effect of flooding water level and plant densityon growth of pneumatophore of Avicennia marina. Tropics 1 (1), 75–82. https://doi.org/10.3759/tropics.1.75.

Twomey, A.J., Lovelock, C.E., 2025. Variation in mangrove geometric traits among genera and climate zones. Estuaries Coasts 48 (2), 55. https://doi.org/10.1007/s12237-025-01487-3.

van Bijsterveldt, C.E.J., Debrot, A.O., Bouma, T.J., Maulana, M.B., Pribadi, R., Schop, J., Tonneijck, F.H., van Wesenbeeck, B.K., 2022. To Plant or Not to Plant: When can Planting Facilitate Mangrove Restoration? [Original Research]. Front. Environ. Sci. 9. https://www.frontiersin.org/articles/10.3389/fenvs.2021.690011.

van Bijsterveldt, C.E.J., Herman, P.M.J., van Wesenbeeck, B.K., Ramadhani, S., Heuts, T. S., van Starrenburg, C., Tas, S.A.J., Triyanti, A., Helmi, M., Tonneijck, F.H., Bouma, T.J., 2023. Subsidence reveals potential impacts of future sea level rise on inhabited mangrove coasts. Nat. Sustain. https://doi.org/10.1038/s41893-023-01226-1.

Van der Stocken, T., Vanschoenwinkel, B., Carroll, D., Cavanaugh, K.C., Koedam, N., 2022. Mangrove dispersal disrupted by projected changes in global seawater density. Nat. Clim. Change 12 (7), 685–691. https://doi.org/10.1038/s41558-022-01391-9.

van Hespen, R., Hu, Z., Borsje, B., De Dominicis, M., Friess, D.A., Jevrejeva, S., Kleinhans, M.G., Maza, M., van Bijsterveldt, C.E.J., Van der Stocken, T., van Wesenbeeck, B., Xie, D., Bouma, T.J., 2023. Mangrove forests as a nature-based solution for coastal flood protection: biophysical and ecological considerations. Water Sci. Eng. 16 (1), 1–13. https://doi.org/10.1016/j.wse.2022.10.004.

van Hespen, R., Hu, Z., Peng, Y., Borsje, B.W., Kleinhans, M., Ysebaert, T., Bouma, T.J., 2021. Analysis of coastal storm damage resistance in successional mangrove species. Limnol. Oceanogr. 66 (8), 3221–3236. https://doi.org/10.1002/lno.11875.

van Maanen, B., Coco, G., Bryan, K.R., 2015. On the ecogeomorphological feedbacks that control tidal channel network evolution in a sandy mangrove setting. Proc. R. Soc. A 471 (2180), 20150115. https://doi.org/10.1098/rspa.2015.0115.

van Oorschot, M., Kleinhans, M., Geerling, G., Middelkoop, H., 2016. Distinct patterns of interaction between vegetation and morphodynamics. Earth Surf. Process. Landf. 41 (6), 791–808. https://doi.org/10.1002/esp.3864.

van Oorschot, M., Kleinhans, M.G., Geerling, G.W., Egger, G., Leuven, R.S.E.W., Middelkoop, H., 2017. Modeling invasive alien plant species in river systems: interaction with native ecosystem engineers and effects on hydro-morphodynamic processes. Water Resour. Res. 53 (8), 6945–6969. https://doi.org/10.1002/2017WR020854.

van Veelen, T.J., Fairchild, T.P., Reeve, D.E., Karunarathna, H., 2020. Experimental study on vegetation flexibility as control parameter for wave damping and velocity structure. Coast. Eng. 157, 103648. https://doi.org/10.1016/j.coastaleng.2020.103648.

van Wesenbeeck, B.K., Wolters, G., Antolínez, J.A.A., Kalloe, S.A., Hofland, B., de Boer, W.P., Çete, C., Bouma, T.J., 2022. Wave attenuation through forests under extreme conditions. Sci. Rep. 12 (1), 1884. https://doi.org/10.1038/s41598-022-05753-3.

Wannasiri, W., Nagai, M., Honda, K., Santitamnont, P., Miphokasap, P., 2013. Extraction of mangrove biophysical parameters using airborne LiDAR. Remote Sens. 5 (4), 1787–1808.

Willemsen, P.W.J.M., Smits, B.P., Borsje, B.W., Herman, P.M.J., Dijkstra, J.T., Bouma, T. J., Hulscher, S.J.M.H., 2022. Modeling decadal salt marsh development: variability of the salt marsh edge under influence of waves and sediment availability. Water Resour. Res. 58 (1), e2020WR028962. https://doi.org/10.1029/2020WR028962.

WWF, 2024. ManglarIA: using artificial intelligence to save mangroves in a changing climate. WWF. Retrieved 21 February from. https://www.worldwildlife.org/projects/manglaria-using-artificial-intelligence-to-save-mangroves-in-a-changing-climate.

Xie, D., Schwarz, C., Brückner, M.Z.M., Kleinhans, M.G., Urrego, D.H., Zhou, Z., van Maanen, B., 2020. Mangrove diversity loss under sea-level rise triggered by bio-morphodynamic feedbacks and anthropogenic pressures. Environ. Res. Lett. 15 (11), 114033. https://doi.org/10.1088/1748-9326/abc122.

Xie, D., Schwarz, C., Kleinhans, M.G., Zhou, Z., van Maanen, B., 2022. Implications of coastal conditions and sea-level rise on mangrove vulnerability: a bio-morphodynamic modeling study. J. Geophys. Res.: Earth Surf. 127 (3), e2021JF006301. https://doi.org/10.1029/2021JF006301.

Yoshikai, M., Nakamura, T., Herrera, E.C., Suwa, R., Rollon, R., Ray, R., Furukawa, K., Nadaoka, K., 2023. Representing the impact of rhizophora mangroves on flow in a hydrodynamic model (COAWST_rh v1.0): the importance of three-dimensional root system structures. Geosci. Model Dev. (GMD) 16 (20), 5847–5863. https://doi.org/10.5194/gmd-16-5847-2023.